Quantifying soil redistribution rates in an agricultural lowland kettle hole in north-eastern Germany by using OSL dating

MSc thesis

Viktoria Vornehm

March 2018

Quantifying soil redistribution rates in an agricultural lowland kettle hole in north-eastern Germany by using OSL dating

MSc Thesis

Viktoria Vornehm
940828905120

Master Earth and Environment,
Soil Geography and Landscape Group

Wageningen, March 2018

Supervisors:

Dr. Tony Reimann

Marijn van der Meij

Prof. Dr. Jakob Wallinga

Cover photo: Young morainic landscape close to the study site in Dedelow, Germany.

Abstract

Soil erosion and redistribution are important processes in agricultural landscapes and the timing of these processes in the past can give insights into driving forces. The closed catchments of kettle holes can provide a complete colluvial record for dating. Three sampling locations in the colluvium of a kettle hole were used for OSL dating. Two of them were located at the edge of the colluvium and one in the center of the colluvium. The aim was to find an OSL dating approach that is suitable for this colluvial setting and to derive ages that can be linked to past land-use. Due to the colluvial setting, poor bleaching of the sediment could be expected. This resulted in the use of a minimum age model (MAM). Three equivalent dose (D_e) analysis approaches were tested and compared. The first approach, which used with the full D_e dataset, gave ages in disagreement with the stratigraphic order. The second approach removed outliers from the D_e dataset and then applied the MAM. The origin of the outliers is either poor bleaching during the transport process or the addition of younger sediment by bioturbation. The third approach used likelihood distributions obtained from the full D_e dataset through Bayesian statistics. These MAM likelihoods were entered in the OxCal program in correct stratigraphic order. Ages resulting from the dataset without outliers and from the OxCal approach differed little. Since OxCal does not require outlier removal and can resolve small inconsistencies of age with depth, it was the preferred data analysis approach.

The OSL ages show that colluviation started around 5000 years ago at the edge of the depression with low sedimentation rates. In the center of the depression, colluviation started in the Middle Ages. High sedimentation rates can be observed from 1800 CE onwards, coinciding with the mechanization of agriculture and hence an increase in tillage erosion.

Contents

List of Figures

1. Introduction

Soil erosion, redistribution and deposition are important processes in sloping agricultural fields, and have been found to be of variable magnitude through time. According to Kleeberg et al. (2016), high redistribution rates coincide with times of intense agricultural use. Soil redistribution is one of the main factors for soil organic carbon distribution on the small landscape scale (Aldana Jague et al. 2016). It is still debated whether soil erosion and deposition act as source or sink of carbon and understanding of the processes in a broad context is needed (Kirkels et al. 2014). Insights into past soil redistribution and its driving forces are of importance for management in agricultural landscapes. The introduction of heavier machinery and intensified cropping systems in the 20th century has increased the contribution of tillage to erosion. Other contributors are water and wind (Kleeberg et al. 2016; Van Oost et al. 2005). Tillage accounted for up to 80% of soil redistribution in the past decades in undulating landscapes (Aldana Jague et al. 2016) resulting in a gradual leveling of the topography (Sommer et al. 2008). The deposited colluvia contain sediment records that form an important geo-archive of past soil erosion, especially in small catchments (Fuchs et al. 2010). These small catchments are very sensitive to changes in land-use (Dotterweich 2008). Soil erosion in central Europe is not only reported for industrial times, but throughout large parts of the Holocene (Dreibrodt et al. 2010). In this longer time frame, deforestation also plays an important role in facilitating soil erosion and colluviation in depressions (Dreibrodt et al. 2010).

For obtaining sedimentation rates, and to see changes in these rates, a complete sedimentation record is required. This is given in locations that form local sediment traps, as is the case for the closed catchments of kettle holes (Sommer et al. 2008; Kalettka et al. 2000) that occur on glacial outwash plains and ground moraines (Maizels 1977). Kettle holes form from melting blocks of buried dead ice and are gradually filled with sediment (Frielinghaus and Vahrson 1998; Maizels 1977). Kettle holes typically contain lakes or peat (Frielinghaus and Vahrson 1998). In central Europe, many kettle holes can be found for example in the young morainic landscape of north-eastern Germany that was deglaciated after the Weichselian glaciation (Kalettka et al. 2000; Sommer et al. 2008; Frielinghaus and Vahrson 1998). Kettle holes are important habitats that show high diversity in species (Kalettka and Rudat 2006). However, with modern large-scale agricultural practices, kettle holes became obstacles and biodiversity declined (Kalettka et al. 2000; Kalettka and Rudat 2006).

Dating the sediment gives quantitative insights into past sedimentation and the obtained ages can be put into perspective with land-use history. Optically stimulated luminescence (OSL) dating allows to directly date the time that passed since the sediment was last exposed to sunlight (Lian and Roberts 2006). OSL makes use of the natural luminescence signal that accumulates over time in mineral grains induced by natural radiation (Preusser et al. 2008). This natural radiation consists of cosmic radiation and radiation emitted from sediment surrounding the sample (Preusser et al. 2008). The accumulated signal is reset when the grain is exposed to sunlight, which is called bleaching (Preusser et al. 2008). The OSL signal in quartz grains are almost completely bleached within 10 seconds (Godfrey-Smith et al. 1988), but if not all grains are sufficiently exposed to light before deposition, poor bleaching occurs. This results in age overestimations if not taken into account. Poor bleaching is an issue in different depositional environments, including colluvial settings (Fuchs and Lang 2009; Preusser et al. 2008). Potential reasons for poor bleaching in colluvia are the small chance of light exposure on a short transport distance, especially in small catchments, and the possibility of movement in blocks, which shields some grains from exposure to daylight (Fuchs and Lang 2009; Preusser et al. 2008). Despite this, OSL dating has been used in a number of studies to successfully date colluvial sediments (Preusser et al. 2008; Fuchs et al. 2010). Fuchs and Lang (2009) postulate two reasons for successful dating: (i) erosion is not one single event, and (ii) mechanical processes like tillage increase the chance of light exposure and bleaching of the grains. Moreover, since colluvia form from many small erosion events (Dreibrodt et al. 2010), bleaching should still be sufficient for OSL dating. In addition to this, bioturbation is an important process that leads to mixing of the topsoil (Wilkinson and Humphreys 2005). This means that prior to erosion, the majority of the grains is already pre-bleached (Reimann et al. 2017).

Kettle holes are found in young morainic landscapes with limited topographic differences. Together with the rather small catchments, this means that sediment is transported only on short distances. These short distances are assumed to be an important contributing factor to poor bleaching of the grains (Fuchs and Lang 2009).

Previous studies dating colluvia were performed at sites with more pronounced topography and showed a link between anthropogenic impacts and Holocene depositional history (Fuchs 2007; Fuchs and Lang 2009; Lang and Hönscheidt 1999). Earlier studies on sedimentation rates in kettle holes found an increase in sedimentation rates after 1955 (Frielinghaus and Vahrson 1998; Kleeberg et al. 2016). These rates are mainly based on concentrations of the man-made ^{137}Cs isotope, which has been released to the environment through nuclear bomb tests from the mid-20th century on (Mabit et al. 2008). Therefore, only very recent sedimentation rates can be obtained from the ^{137}Cs isotope; information on longer time spans is not available from dating with ^{137}Cs (Mabit et al. 2008). The use of ^{14}C dating in colluvia is also difficult due to the reworking of sediment and organic material (Lang and Hönscheidt 1999; Zolitschka et al. 2003). Therefore OSL offers an alternative without the time resolution constraints of ^{137}Cs and the reworking issues associated with ^{14}C dating.

Based on the information available from ^{137}Cs dating in kettle holes, and the problems with poor bleaching in a colluvial sediment, three goals arose for this thesis:

- To find an OSL dating approach that is suitable for dating of a colluvial deposit in a young morainic landscape
- To derive OSL ages and sedimentation rates for an agriculturally used kettle hole
- To link the obtained OSL ages and sedimentation rates to human impacts on the landscape

Hypotheses are, that the OSL measurements are influenced by poor bleaching due to the colluvial setting of the kettle hole sediments. Furthermore, it is expected that the OSL ages of the colluvium do not date back further than the Middle Ages and that sedimentation rates increased with the mechanization of agriculture. It is also hypothesized that the measured OSL distributions per sample contain information on the transport process, as this influences the bleaching of the grains.

2. Study area

The study area is located close to the village of Dedelow in north-eastern Germany. The rural region called "Uckermark" lies approximately 100km north of Berlin. The sampling location is situated in the CarboZALF-D site, which is a kettle hole catchment.

2.1. Geomorphologic and pedologic setting

During the Weichselian, the Uckermark region was glaciated. The region became ice free after the Pomeranian stage of the glaciation which is dated to around 20ka (Lüthgens et al. 2011). According to Lüthgens et al. (2011), previous surface exposure dating in the region showed that a first stabilization of the landscape after melting of dead ice bodies took place around 16.5ka ago and intensified with the beginning of the Bølling interstadial. Deglaciation and melting of the dead ice left an undulating ground moraine landscape where many kettle holes can be found irregularly distributed (Kalettka et al. 2000). Today, there is an estimated number of 150,000 to 300,000 kettle holes in the young morainic landscape of north-eastern Germany (Kalettka and Rudat 2006). According to Kalettka et al. (2000), this number has halved since the turn of the 20th century, as kettle holes were a hindrance for large-scale agriculture. Within this landscape, the study area is situated (Figure 1A).

The Uckermark region mainly is covered by soils that developed in glacial deposits, with clayey sediments in the ground moraines and part of the end moraines, and sandy material in parts of the end moraines and on the sandr areas (Figure 1B). Moreover, the region is characterized by a number of glacial valleys that are north-south orientated, and where many rivers and lakes are located presently.
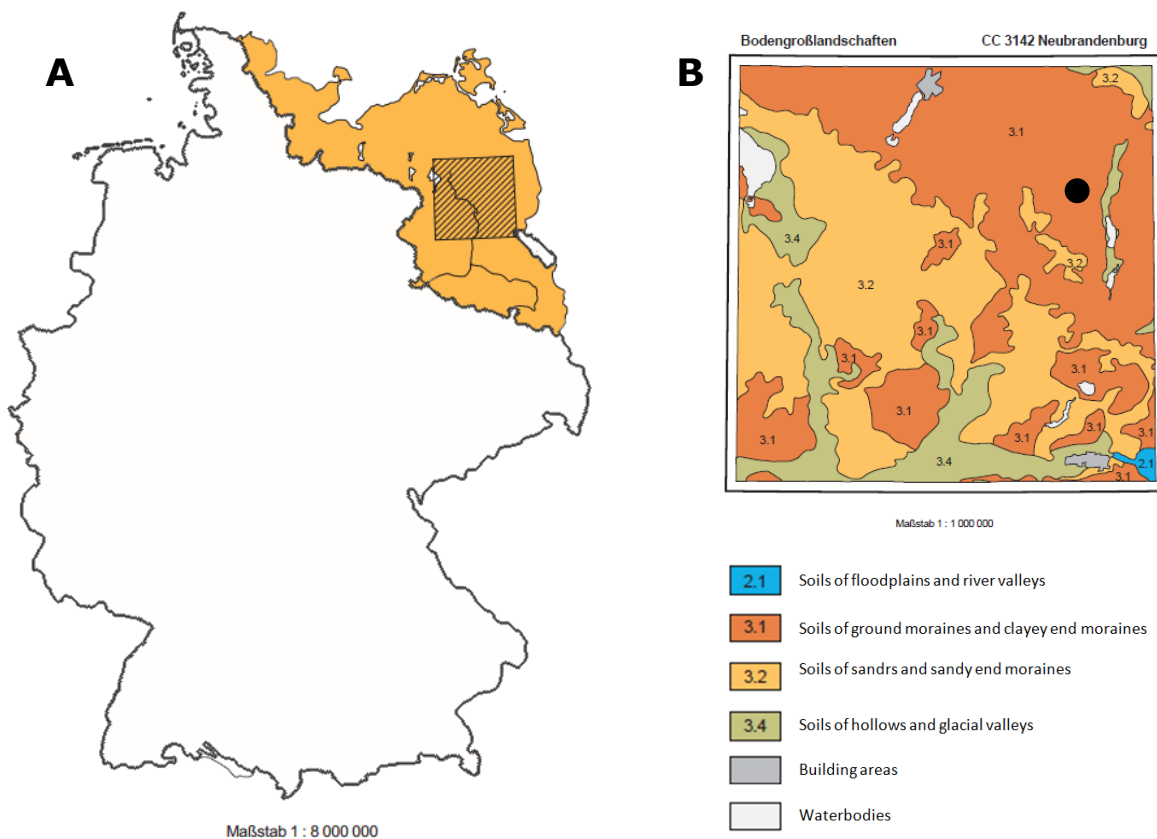
Figure 1: *Illustration of the extent of the young morainic landscape of north-eastern Germany marked in orange (**A**). **B** shows the large soil landscapes that are found in the region around the study site. The field site (black dot) is located within the ground moraine and clayey end moraine unit. Modified from BGR (2015).*

Within the closed catchments of the kettle holes, different soils have developed. Under natural conditions, without erosion and deposition, the wet center of the kettle holes contain Histosols, whereas Luvisols are present on the slopes (Van der Meij et al. 2017). Due to erosion however, sediment was deposited in the center of the depression, resulting in a soil classified as Endogleyic Colluvic Regosol (Van der Meij et al.

2017). On the eroded slopes, the classification depends on the severity of the erosion. Albic Luvisols are found if little erosion took place, Calcic Luvisols are found where the soil was strongly eroded and Calcaric Regosols are found where erosion had been most extreme (Van der Meij et al. 2017).

The soils of the colluvium contain a buried A horizon (fAh) which marks the level of the former land surface (Frielinghaus and Vahrson 1998). This fAh formed either in the glacial till or in the peat in the center of the depression. Above this fAh lies the colluvium, referred to as M horizon. The top of the colluvial horizon is located within the current ploughing depth of 30cm and forms the Ap horizon.

2.2.   Regional land-use history

Pollen profiles from lakes provide records on past agricultural use in the region (Jahns 2001). These reveal significant anthropogenic impact since Neolithic times, starting around 4000 BCE (Jahns 2000). The most intense historical human impact coincides with an opening of the woodlands between 3200 and 1900 BCE (Jahns 2001). Dreibrodt et al. (2010) reports this phase to be present throughout Central Europe. Another phase of intense human impact took place between 1440 and 500 BCE (Jahns 2000). This time coincides with reports of large scale forest clearance for the region around the Unteruckersee (Jahns 2001). The pollen profiles show that human activity decreased in the following Roman Iron Age and the Migration period (Jahns 2000, 2001), which came along with large-scale forest cover in Germany (Dotterweich 2008).

The land-use intensity since Early Medieval times is higher than earlier human activities in the region (Jahns 2000). This high land-use intensity was preceded by large-scale forest clearance (Jahns 2000). By the early 14th century, large parts of Germany consisted of arable land and high occurrences of colluvial sediments are reported (Dotterweich 2008; Dreibrodt et al. 2010). The deforestation contributed to erosion, as it locally caused severe water erosion during heavy rainfall events (Sommer et al. 2008). 1320 CE, Dedelow which developed from a previous Slavic settlement is first mentioned (Wolff 2018). The region around Dedelow has also been used agriculturally since medieval times (Sommer et al. 2008). This long agricultural use has influenced the landscape for example by causing soil redistribution in the kettle holes (Frielinghaus and Vahrson 1998).

In the 18th and 19th centuries, agrarian structuring and reformations all over Central Europe resulted in measures to improve the land suitability for agriculture, for example by implementing drainage (Kleeberg et al. 2016; Dotterweich 2008). After the Second World War, agricultural production cooperatives were founded and small fields were collectivized (Sommer et al. 2008; Bayerl 2006). Most structures inhibiting erosion were removed in this course to create large arable fields (Kleeberg et al. 2016; Bayerl 2006). Within these large, industrialized agricultural units (Kleeberg et al. 2016), the kettle holes became a hindrance. Filling of kettle holes led to a leveling of the topography (Kalettka et al. 2000; Bayerl 2006; Sommer et al. 2008). Deeper ploughing in the 1970's and 80's increased erosion even more (Sommer et al. 2008). Currently, 63% of the Uckermark region are agriculturally used, with mainly cereal being cultivated (Kleeberg et al. 2016).

2.3.   CarboZALF-D study site

The CarboZALF-D study site is an experimental field that is operated by the Leibniz Centre for Agricultural Landscape Research (ZALF). The field site is used for a number of experimental studies, which mostly focus on the link of tillage and erosion with carbon cycling in the soil. These studies include for example a manipulation experiment that aimed at the influence of erosion on carbon dynamics in the soil (Deumlich et al. 2017). During a study on soil organic carbon variability, ^{137}Cs measurements were made in the CarboZALF-D site, which found that between 1954 and 2011 a maximum of 27cm of sediment was deposited in the kettle hole (Aldana Jague et al. 2016). Although a lot is known about this field, no information was available on the longer scale temporal aspects of landscape development.

The kettle hole of the field site contains a buried peat layer with a fossil Ah horizon. The sediments above the fAh are all part of the colluvium. At present, the colluvium in the CarboZALF-D kettle hole is up to 1.8m thick (Van der Meij et al. 2017). At the base of the colluvium above the peat, an oak stem has been found that was dated to 1306 ± 10 CE (Van der Meij et al. 2017), which provides a first indication of the age of the colluvial sediments. In the colluvium, Colluvic Regosols are found, whereas on the eroding slopes Albic or Calcic Luvisols are present (Van der Meij et al. 2017). The field site is regularly ploughed.

3. Methods

Different methodological steps were taken to obtain OSL ages and sedimentation rates. Figure 2 provides a workflow through the methodology. Further explanations are given in the following sections.
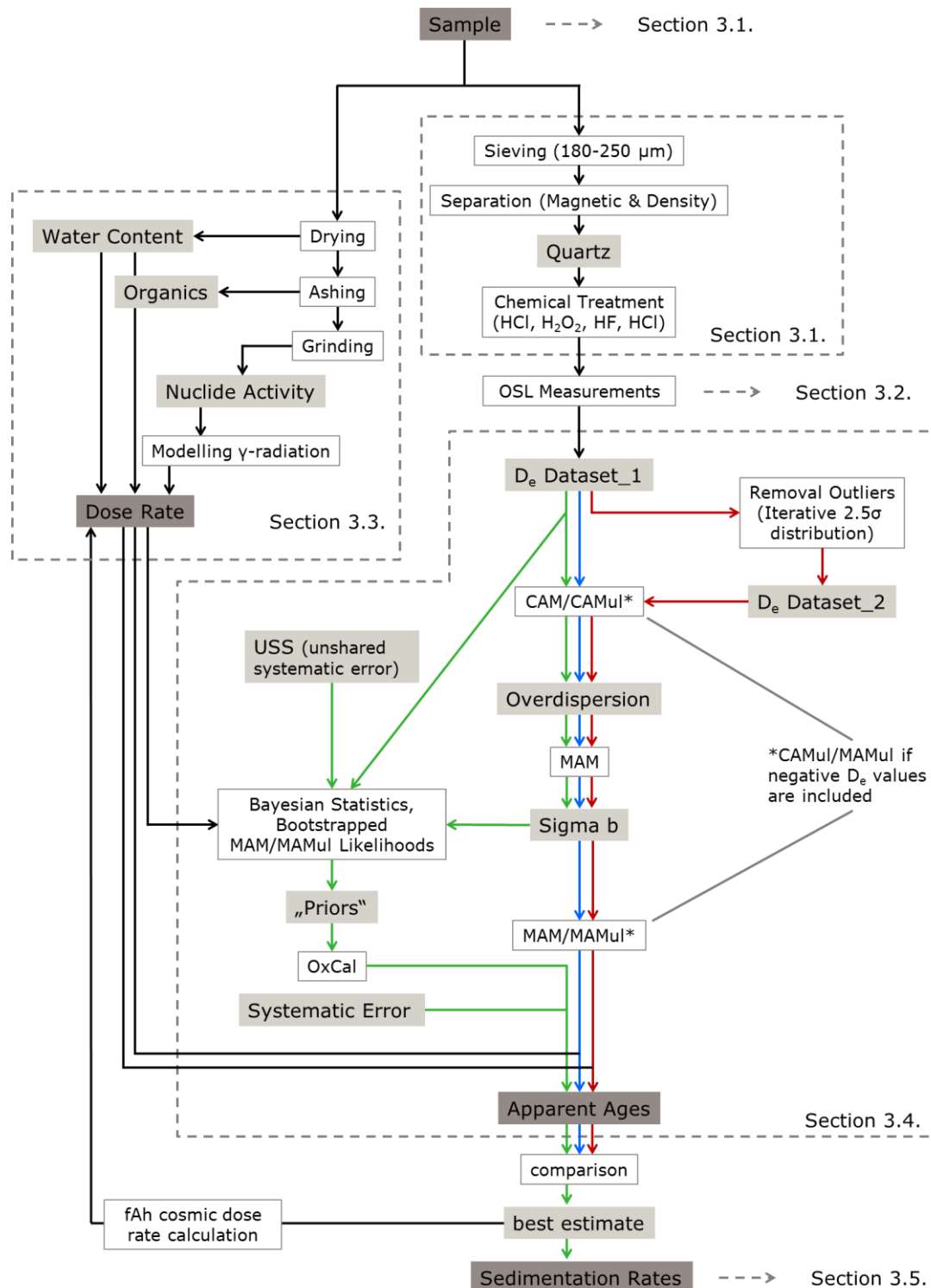
Figure 2: Workflow of sample preparation, measurements, data analysis and the final model selection. The framed parts are described in further detail in the respective section of this thesis. The different colors in section 3.4 (Dₑ analysis) refer to the three different analysis approaches: Blue results in the MAM_1 ages, red in the MAM_2 ages and green in the OxCal ages. These ages were then compared to each other to determine the best estimate. White boxes are methodological steps, light grey boxes show intermediate results and the dark grey boxes present the main results.

3.1.   Sample collection and preparation

3.2.1. Sampling locations

Fieldwork for sample collection took place in April 2017. Two soil pits (P2 and P3) were situated at the slopes of the depression (Figure 3). Core BP5 was located in the center of the depression, where the deepest colluvium was expected. This core was therefore expected to contain the most complete sediment record.
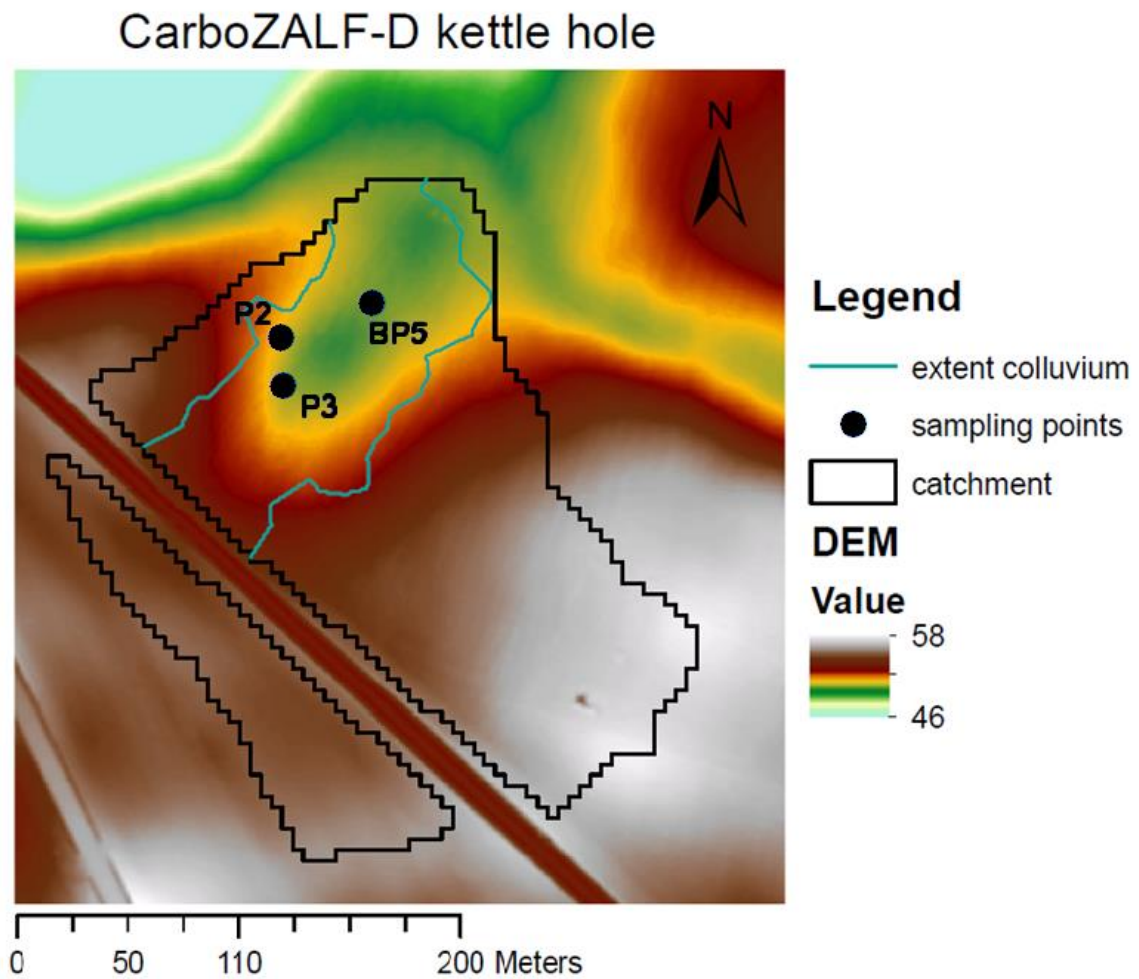

Figure 3: *Digital elevation model of the study site, showing the kettle hole, the three sampling locations and the expected extent of the colluvium. The catchment is split by a former railway track.*

P2

P2_12
P2_30
P2_40
P2_50
P2_60
P2_70
P2_85

P3

P3_30
P3_70

BP5

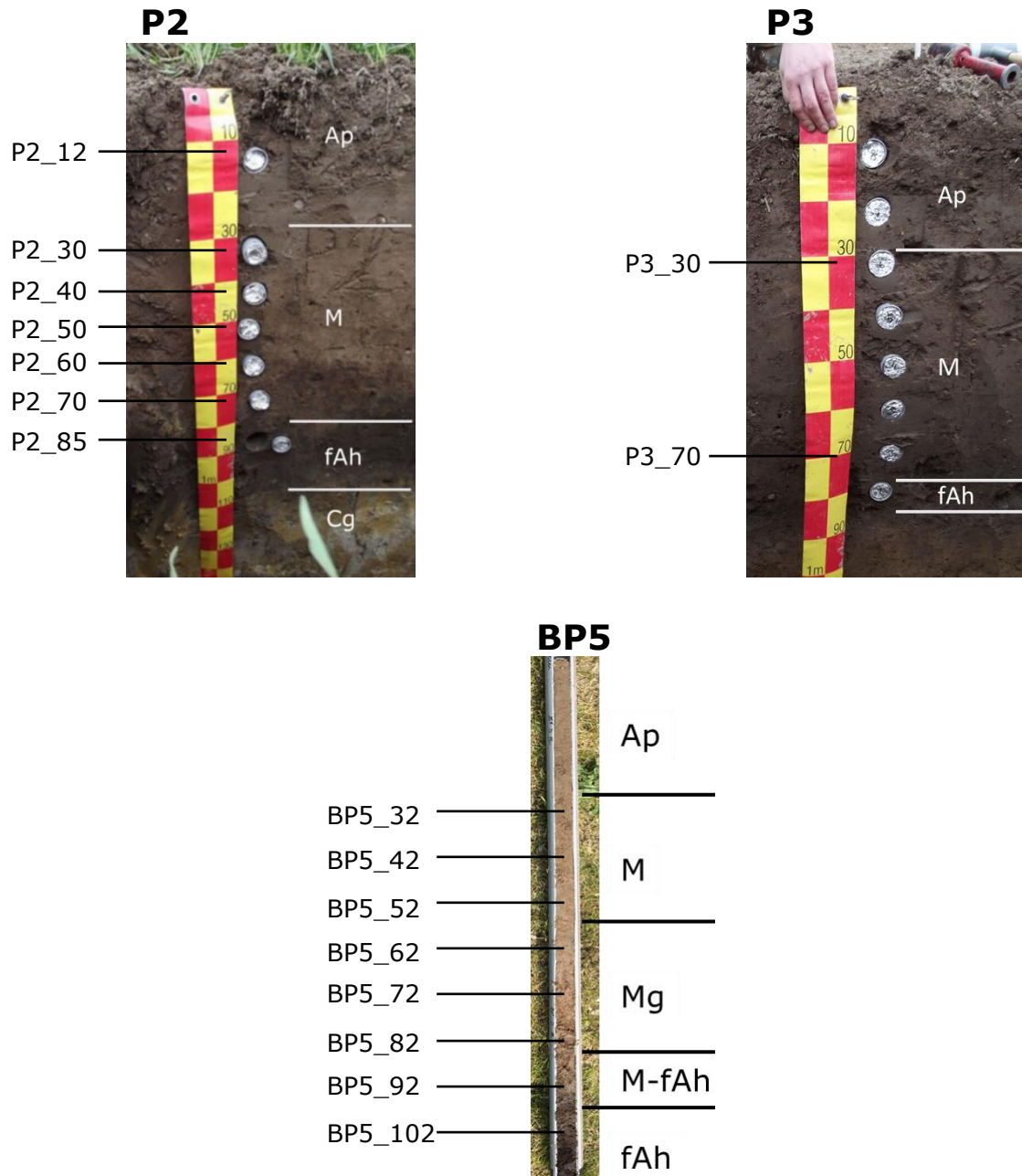BP5_32
BP5_42
BP5_52
BP5_62
BP5_72
BP5_82
BP5_92
BP5_102

Figure 4: Soil profiles of the three sampling locations with soil description on the right hand side with "M" referring to the colluvium. The sample codes are presented on the left of each profile, and consist of the profile code and the upper depth of the OSL sample.

The horizontal OSL samples in the soil pits (P2 and P3) were taken by hammering 20cm long, lightproof PVC tubes with a diameter of 5cm into the wall of the soil pit. The lowest samples were taken in the fAh horizon. In the M horizon above the fAh, OSL samples were taken every 10cm (Figure 4). The ploughing horizon (Ap) was also sampled, although this horizon is regularly mixed and bleached due to agricultural practices. This sampling strategy was applied to both soil pits. For BP5, three 2m long vertical cores were taken. The distance between these three was 0.5m in a triangle. One of the three cores was sampled every 10cm in the subdued light conditions of the NCL laboratory. The other two cores were used to obtain sediment for dose rate measurements and to describe the soil profile. Not all samples taken were analyzed for this thesis project, but were kept for possible later dating and analysis. An overview of all samples taken is presented in Table 1.

Table 1: Overview of the sampling locations with the corresponding fAh depth, the number of samples taken from the profiles and the number of samples used for OSL dating.

	Location	Samples	Dating	Remarks	Depth fAh [cm]
Pit P2	Slope, small upslope area	7	7	Complete profile	75
Pit P3	Slope, large upslope area	8	2	Lowest and highest colluvium	78
Core BP5	Center of depression	10	8	All except the Ap horizon	100

3.2.2. Sample preparation

Sample preparation of the horizontal tubes started with splitting the material into equivalent dose (D_e) material, hence the luminescence signal of the grains, and dose rate (DR) material. The DR is the annual amount of natural radiation that the sample was exposed to during burial (Preusser et al. 2008). The outside 3cm on both sides of the tube were used for DR measurements (Figure 5) as this part of the tube was exposed to light during the field sampling.
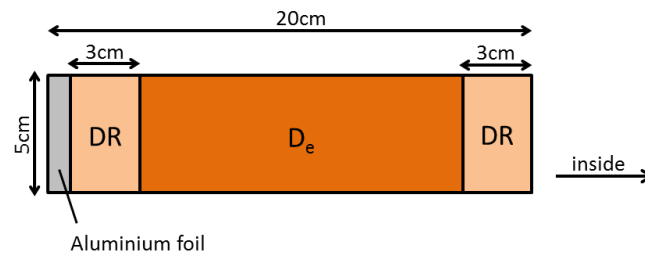

Aluminium foil

Figure 5: Scheme illustrating how the material in the horizontal OSL tubes was split into D_e and DR material. The inside arrow indicates where the soil profile wall was located in the field. Aluminum foil was used on the outside to prevent soil material from tumbling during hammering.

For the vertical core, laboratory work started with sawing the PVC core open and taking D_e material every 10cm. To prevent contamination, it was taken care that no material from directly at the core wall was included (Figure 6). This material from the wall and directly above and below the sample was used as DR material (Figure 6). Since there was not enough DR material from two half cores alone, material from the respective depth from a second core was added.
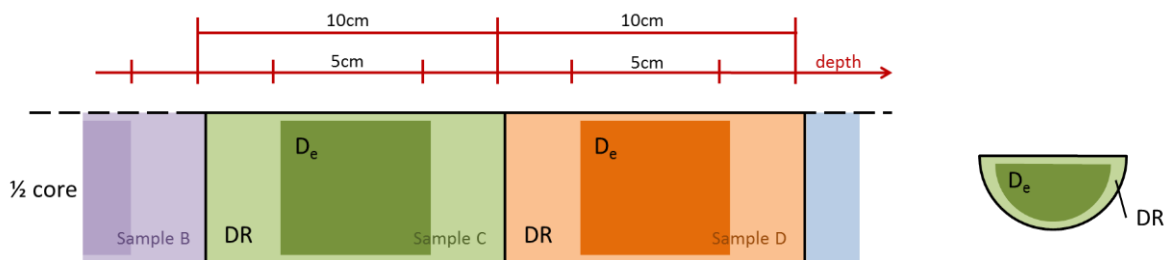

Figure 6: Sampling scheme for the vertical soil cores on the left, with a cross section on the right hand side. The same scheme was used for the complete depth of the core.

The D_e material was first wet sieved over sieves of 250μm, 180μm and 90μm. The 180-250μm fraction was chosen for the measurements, because larger grain sizes allow for better control of the number of grains on an aliquot. This is of importance, as larger aliquots with many grains contributing to the bulk luminescence signal will show an averaging of the measured D_e values (Duller 2008). In settings with expected poor bleaching, this averaging from multiple OSL signals on one aliquot results in an over-estimation of the age. After sieving, the material was chemically treated with HCl and H_2O_2 to remove carbonates and organic matter. Subsequently, the material was density separated into quartz and feldspar

fractions. Only the quartz fraction was used further. The quartz grains then were treated with HF to remove remaining feldspars and to etch the outer rim of the grains that are affected by radiation (Preusser et al. 2008). After this treatment, the quartz grains could be mounted on stainless steel discs for D_e measurement (Section 3.3).

The DR material was dried overnight at 105°C to determine the water content of the sample. Further, the material was ashed to obtain the organic matter content. After grinding the material to a size smaller than 300μm, sediment and wax were mixed in a 70% sediment to 30% wax ratio and 2cm thick pucks were molded. If not enough sediment was available, a 1cm puck was prepared with the same sediment to wax ratio.

3.2.   Equivalent dose measurements

For luminescence measurements, the quartz grains were mounted on stainless steel discs using silicone spray. Prior to D_e measurements, the following tests were performed to get insight into the characteristics of the quartz grains. Firstly, an IR test was conducted with large aliquots (5mm) to check for feldspars in the material. Secondly, a Thermal Transfer Test on large aliquots (5mm) was performed on three of the samples. Thermal transfer refers to a signal that is created due to the thermal preheating of the aliquots which can result in charge moving from light insensitive to light sensitive traps (Madsen and Murray 2009). Based on the result of the Thermal Transfer Test, preheat temperature of 200°C and a cutheat temperature of 180°C was used. Lastly, a Dose Recovery Test was performed to confirm the chosen measurement settings. This test was first performed on aliquots of 2mm mask size. For the Dose Recovery Test, 47 of the 108 measured discs were accepted. The average Dose Recovery Ratio was 1.01 ± 0.02 and all accepted discs fell within the uncertainty bands around a ratio of 1 (Figure 7).
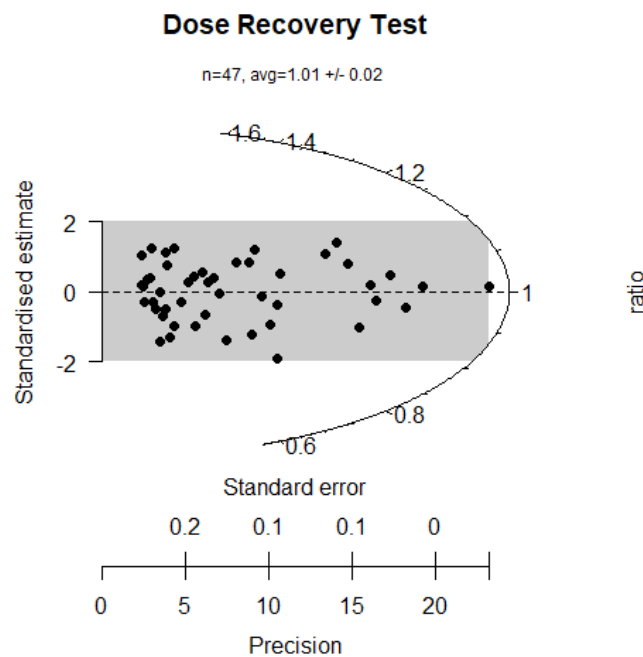
Figure 7: Radial Plot according to Galbraith (1990) of the Dose Recovery Test results with the ratio on the radial z-axis. All 47 accepted measurements lie within the uncertainty bands and therefore validate the chosen measurement setup with preheat- and cutheat temperatures of 200°C and 180°C respectively.

Since more than 70% of all discs were accepted on the 2mm aliquots of the Dose Recovery Test, a 1mm mask size with less strict acceptance criteria was chosen instead. The selected acceptance criteria for the discs were:

- recycling ratio ≤ 20%
- test dose error ≤ 20%
- recuperation ≤ 10%

D$_e$ measurements were then performed following the SAR protocol proposed by Murray and Wintle (2003).

With these settings, 31% of the measured discs were accepted. The percentage of accepted aliquots per sample is provided in Appendix Table A3. With roughly 15-20 grains per disc, the results were almost at the level of single grain measurements. This is supported by previous single grain OSL measurements in the study region that found roughly 4% of the measured quartz grains to be accepted (Lüthgens et al. 2011).

3.3.   Dose rate measurements and analysis

The nuclide activities per sample were measured by gamma ray spectrometry. The measured nuclide activities were then converted to beta and gamma dose rates by using the conversion factors of Guérin et al. (2011). The DR then was calculated under consideration of the radiation attenuation by water and organic matter contents. Organic matter and water contents were determined per sample as described in Section 3.2 and are provided in Appendix Table A2. This is of importance, as both water and organic matter absorb beta and gamma radiation (Madsen et al. 2005). Furthermore, grain size dependent attenuation of beta radiation (Mejdahl 1979) and the depth below surface for the cosmic dose rate component were taken into account (Prescott and Hutton 1994).

The gamma radiation components of the different samples interfere with each other, as gamma radiation has a penetration distance of a few decimeters (Preusser et al. 2008). This is larger than the distance between the samples, which in most cases is 10cm. The contribution of the samples within 42cm of the sample itself were taken into account by using the attenuation factors by Aitken (1985) that increase with distance from the sample. The sum of the different contributions gave the gamma radiation component per sample.

As the presence of an fAh horizon indicates a longer period of stable conditions, samples taken in this horizon have been close to the surface for a longer time. This has an impact on the cosmic dose rate component, as at the surface no sediment layer is present to absorb cosmic rays (Madsen et al. 2005). To calculate the cosmic dose rate of the fAh (*cosm. DR$_{fAh}$*), this period of high cosmic radiation exposure of the fAh samples was taken into account by assigning a burial depth of 5cm to the sample for the time until the lowest colluvium sample was deposited (*cosm. DR$_5$*). For the remaining time until sample collection, the cosmic dose rate of gradual burial with the final depth (*x*) was used (*cosm. DR$_x$*). This calculation step could only be taken, after the ages of the fAh and lowest colluvial sample were known (*Age fAh* and *Age M*). Hence this cosmic dose rate calculation was a loop in the D$_e$ analysis (Figure 2). Resulting from the newly calculated total cosmic dose rate, the age of the sample can change. Therefore, this calculation was repeated until the age didn't change anymore. Equation 1 demonstrates the calculation for the cosmic dose rate component of the fAh.

$$cosm.\ DR_{fAh} = cosm.\ DR_5 * \frac{Age\ fAh - Age\ M}{Age\ fAh} + cosm.\ DR_x * \frac{Age\ M}{Age\ fAh} \qquad (1)$$

3.4.   Equivalent dose analysis

Due to the colluvial setting of the study site, there is a possibility of insufficient light exposure of the grains at deposition. This poor bleaching has to be taken into account during the D$_e$ analysis. Therefore, the age model of choice is a minimum age model (MAM) (Galbraith et al. 1999). However, since some of the very young samples include negative D$_e$ values, the unlogged version of the minimum age model (MAMul) needs to be used for these cases. Due to the poorer performance of the MAMul (Arnold et al. 2009), it was chosen to use the logged MAM whenever possible. In the workflow, no difference was made between results obtained from the logged and the unlogged versions of the age models (Figure 2). In order to apply the bootstrapped MAM/MAMul, overdispersions (ODs) were first determined by applying a central age model (CAM) (Galbraith et al. 1999) to each samples' D$_e$ distribution (Figure 2). These ODs show the spread in the distribution that is not explained by experimental uncertainties (Arnold et al. 2009; Lian and Roberts 2006). Therefore, higher ODs should be linked to distributions including more outliers and/or being affected by poor bleaching or post-depositional mixing. The OD value that could be expected for a perfectly behaving natural sample without influence of poor bleaching or post-depositional mixing, is referred to as sigma b (e.g. Cunningham and Wallinga 2012). This sigma b is determined by applying a MAM to the ODs and is used as input for the bootstrapped MAM.

To obtain palaeodoses and ages from the D_e distributions, three different approaches, described in the following, were tested.

1. MAM_1
   The full D_e distribution per sample (referred to as D_e Dataset_1, Figure 2) was used to obtain OD and a sigma b value, which was an input for the bootstrapped MAM/MAMul.

2. MAM_2
   The second approach included a step of outlier removal. Based on the D_e distributions, all single D_e measurements outside of 2.5σ were removed. Since the broadness of a distribution depends on the single measurements in it, the outlier removal procedure was repeated five times per sample. 2.5σ was chosen as this value removed most outliers that were visible to the eye. The new dataset without outliers, referred to as D_e Dataset_2 (Figure 2), then was used in the same way as D_e Dataset_1 for determining a new sigma b value from the new ODs. Finally, the bootstrapped MAM/MAMul was applied again to obtain palaeodoses, which divided by the DR results in age.

3. OxCal
   The third approach was based on using the full D_e Dataset_1, and the sigma b value of Dataset_1 like for the MAM_1 approach. This time, bootstrapped likelihoods were calculated in MatLab from the D_e data, as described by Cunningham and Wallinga (2012). Further inputs for the likelihoods were the DR per sample, and the unshared systematic error (USS), as described by Rhodes et al. (2003). The obtained likelihood distributions, further termed "Prior", then were used as input for the program OxCal. This program is originally developed for the analysis of radiocarbon dates with the possibility of combining ages with stratigraphic information or dates obtained from other dating techniques (Ramsey 1995). OxCal uses Bayesian statistics to determine the most likely age distribution per sample (Ramsey 1995, 2008), called "Posterior". OxCal version 4.3.2. was used for analysis. The so called *P_Sequence* was chosen, which takes the stratigraphic order of the samples and the Prior as input. The output given by OxCal does not encompass shared systematic errors and these were included after the OxCal simulation (Rhodes et al. 2003). An indication of how well the Posterior fits the Prior is given by the agreement factor A provided by OxCal. Generally, an agreement factor below 60% is regarded as indication of the sample being in the wrong stratigraphic position (Ramsey 1995). The 60% threshold level is based on statistical confidence levels (Ramsey 1995).

3.5. Sedimentation rates

Changes in sedimentation rates can provide insights into phases of intensified erosion. This is of interest for placing sedimentation and erosion in a context of anthropogenic impact. The different sets of ages from the three approaches (Section 3.4.) were further compared to each other, and the approach offering the best age estimate was used for sedimentation rate calculations. The sedimentation rates were obtained from combining the age difference and depth (X) difference between two consecutive samples A and B (Equation 2). Next to the age error (δAge), also a depth error (δX) of 1cm was included in the calculations, leading to a sedimentation rate error through error propagation (Equation 3):

$$Sed.\,rate = \frac{X_B - X_A}{Age_B - Age_A} \qquad (2)$$

$$Sed.\,rate\,error = Sed.\,Rate * \sqrt{\left(\frac{\sqrt{\delta X_B^2 - \delta X_A^2}}{X_B - X_A}\right)^2 + \left(\frac{\sqrt{\delta Age_B^2 - \delta Age_A^2}}{Age_B - Age_A}\right)^2} \qquad (3)$$

The sedimentation rate from the uppermost sample to the surface was calculated by including zero depth and zero age for the surface. In order to make a comparison to previous studies in kettle lakes (e.g. Frielinghaus and Vahrson 1998; Kleeberg et al. 2016) that calculated sedimentation rates before and after 1955 based on ^{137}Cs, the sedimentation rates were also calculated for this time.

4. OSL ages

Three different approaches are tested and compared to each other to obtain OSL ages of the colluvium. In this chapter, the results of the OSL measurements are presented and discussed. Further, the three analysis approaches are compared to each other. With the D_e analysis approach giving the best age estimate, sedimentation rates for the different profiles are calculated. The interpretation of the obtained ages and the link to landscape changes is provided in chapter 5.

4.1. Soil profiles

The pedological setting of the different samples gives information on past soil formation and hence on past conditions. The formation of an fAh horizon is an indicator of past stable land surface (Frielinghaus and Vahrson 1998) where erosion and deposition therefore are absent (Emadodin et al. 2011). The two samples taken in the fAh at the edge of the colluvium and in the center of the depression show differences in organic matter content. The fAh at the edge of the colluvium is of mineral origin with an organic matter content of 2%, which is not higher than in the overlying colluvium. The organic matter content in the depression fAh in contrast to the slope is 40% (Appendix Table A2). A more detailed soil description per profile is presented in Figure 5 and Appendix Table A1.

4.2. Overdispersions

The ODs provide further information on the sample. From the ODs of all 17 samples, the sigma b value which is further used in the analysis is obtained by applying the MAM to the ODs. The ODs show a lot of variation between the individual samples, ranging from as low as 4 ± 4% to as high as 72 ± 24% in Dataset_2 (Appendix Table A3). The ODs of Dataset_2 are smaller compared to Dataset_1 due to the outlier removal. As the ODs decrease by removing outliers, also the sigma b value decreased, 18 ± 5% for Dataset_2 compared to 28 ± 3% for Dataset_1. However, the sigma b value in both datasets is supported by the same amount of ODs (Figure 8, grey bars).
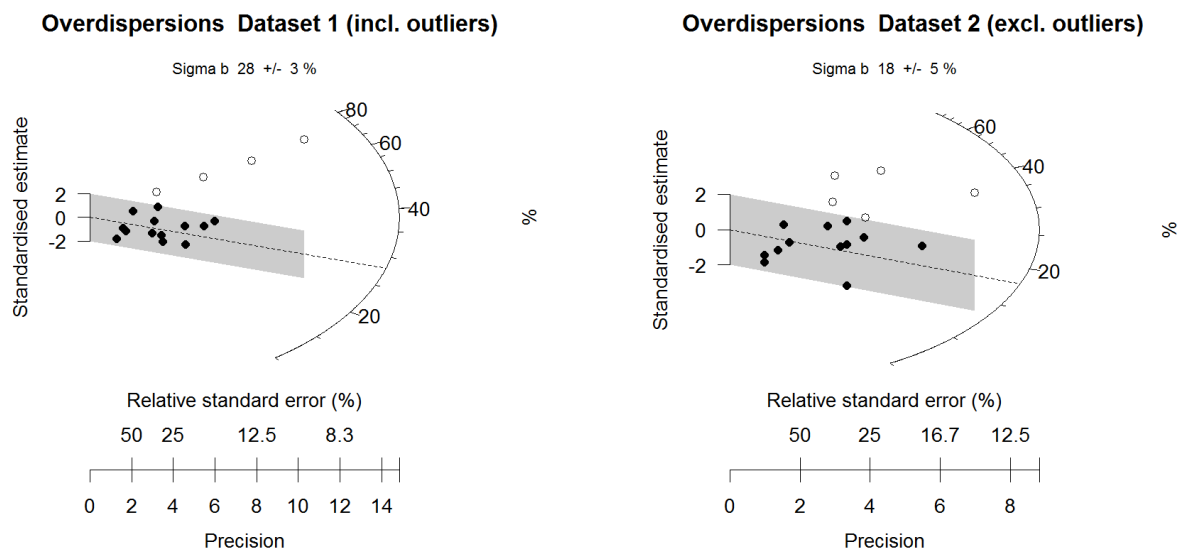

Figure 8: Radial plots showing the ODs of the 17 individual samples plotted with a MAM which results in the sigma b value. The left graph presents the ODs and sigma b value of D_e Datset_1, the right side presents the results of D_e Dataset_2 where outliers had been removed.

4.3. D_e distributions

The D_e distributions consist of 23 to 33 accepted discs for the different samples. The distributions of four samples are discussed in more detail to give an indication of the distributions resulting from the D_e measurements. KDE plots and radial plots (Galbraith 1990) for all samples are provided in Appendix Figures A1, A2 and A3.

Firstly, most of the D_e distributions present older outliers indicating insufficient OSL signal resetting of some grains (Figure 9A), which was expected for this colluvial setting. Values above 20Gy are not found

in core BP5, but occur several times at different depths in soil pits (e.g. P2_85, P2_60, P3_70). The absence of very old outliers (>20Gy) in BP5 indicates that the colluvium in the center of the depression is better bleached than at the edge of the depression. Reworking of the sediment is a possible explanation for this. In this first type of D_e distributions, the MAM is very well supported by the D_e measurements, as can be seen from the grey confidence band in the radial plot (Figure 9A). This is also in agreement with the very small OD that results from analysis of D_e Dataset_2 of 4 ± 4%, which is in the range of well bleached aeolian samples (Rodnight et al. 2006). The small OD for Dataset_2 is caused by the outlier removal, as grains with clear insufficient bleaching fall outside the 2.5σ distribution.

Secondly, two of the D_e distributions, P2_70 and P2_60, also contains very young D_e measurements with values close to 0Gy (Figure 9B). Especially at the depth of 60 and 70 cm, this was unexpected. Causes for these values could be post-depositional mixing through bioturbation or possible contamination during sample preparation. These outliers have a large influence on the MAM, if applied to the full D_e Dataset_1. These D_e measurements were removed for D_e Dataset_2 using the outlier removal procedure described in Section 3.4.

The third type of D_e distribution had no outliers determined for removal for D_e Dataset_2. This is the case for very broad distributions like for P2_40 (Figure 9C). These D_e distributions show ODs, up to 72 ± 24% for D_e Dataset_2, which means that they have a large spread that cannot be explained by experimental uncertainties. The MAM in these cases is supported by only few of the individual D_e measurements (Figure 9C).

The Ap horizon, P2_12, (Figure 9D) shows the fourth type of D_e distribution that has undergone recent reworking by ploughing and does not show the depositional age of the colluvial sediment. Hence it is no surprise that the MAM gives a result close to 0Gy. The KDE plot of P2_12 reveals that there are still a number of grains measured with higher D_e values, that had not been bleached even though the sample is situated in the Ap horizon. Additionally, P2_12 is taken from the part of the profile exposed to most bioturbation (Reimann et al. 2017). A very similar pattern of D_e distributions can be seen as well for samples P2_30 and P3_30 just below the Ap horizon (Appendix Figure A1).
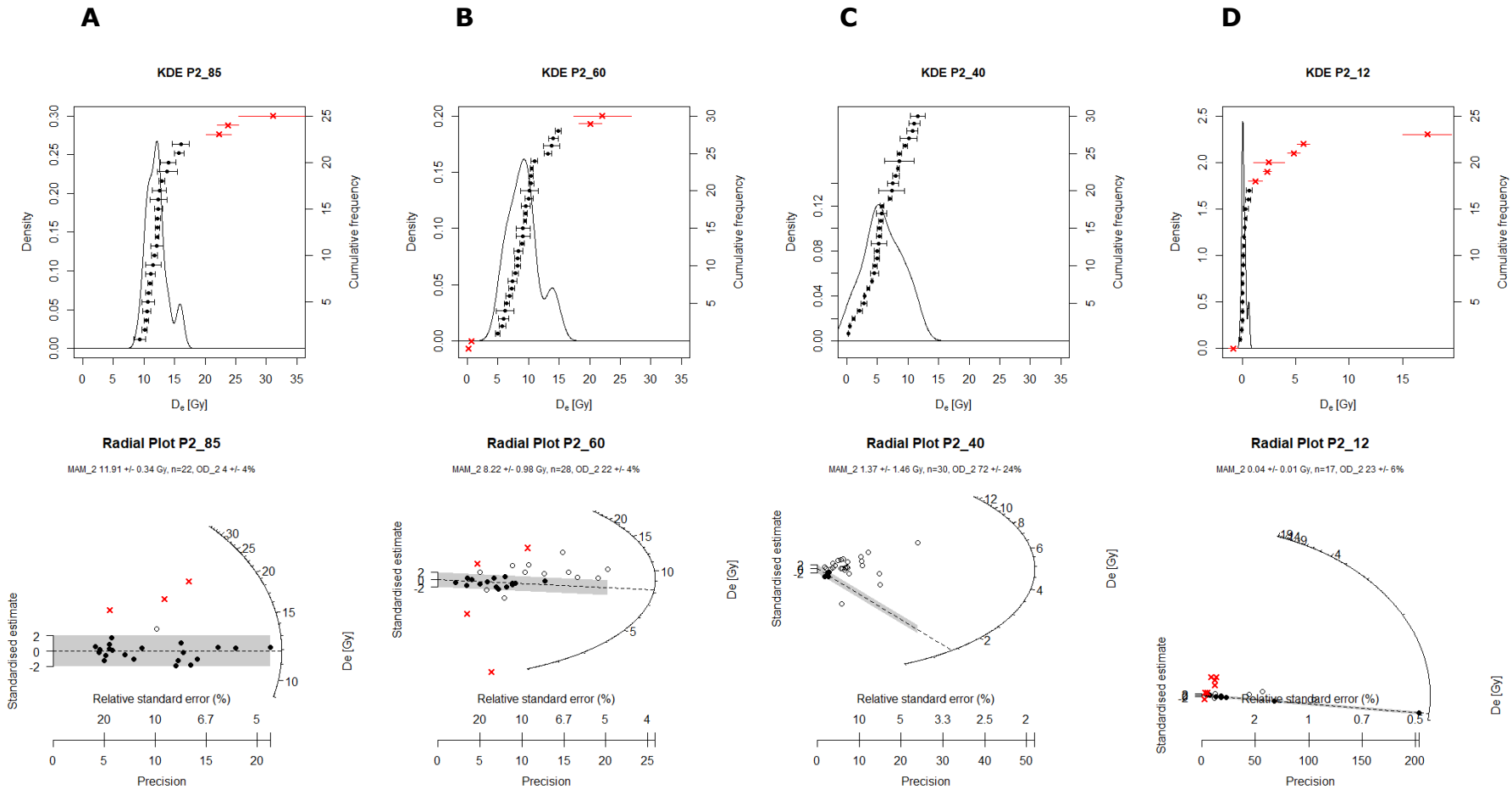
Figure 9: *KDE plots and radial plots of the different D_e distributions found after measurements. The outliers, both poorly bleached grains and measurements influenced by post-depositional mixing, removed for D_e Dataset _2 are marked with red x in the graphs. The radial plot gives the D_e measurements supported by the MAM applied to D_e Dataset_2 (grey confidence bands) and the OD resulting from D_e Dataset_2. **A** presents a sample (P2_85) with clear signs of poor bleaching. Outliers are only found at the old end of the D_e distribution. **B** shows sample P2_60 with both old and very young outliers (around 0Gy), that strongly influences the MAM. **C** presents the D_e distribution and radial plot of a sample (P2_40) with a very high OD, where no outliers can be identified by the chosen approach. Also, the MAM is only supported by very few measurement points. **D** presents sample P2_12 from the ploughing horizon. The distribution clearly shows that the majority of the D_e measurements are very young and only few of the measurements have higher D_e values.*

4.4. Choice of age model

A comparison of the results for CAM and MAM per sample gives an indication for the differences between these two age models. For a number of the samples, the differences are minor and the CAM/MAM ratio lies around 1 (Figure 10). Other samples however show a large CAM/MAM ratio. The most extreme case is the sample from the ploughing horizon (P2_12) which gives a CAM/MAM ratio of more than 40 for D_e Dataset_1. This, in addition to the poor bleaching visible from the D_e distributions (Figure 9A), supports the choice of the MAM for D_e analysis. It can also be seen in Figure 10 that higher CAM/MAM ratios are associated with larger ODs. Furthermore, ODs and CAM/MAM ratios decrease due to outlier removal as applied for the second D_e analysis approach.
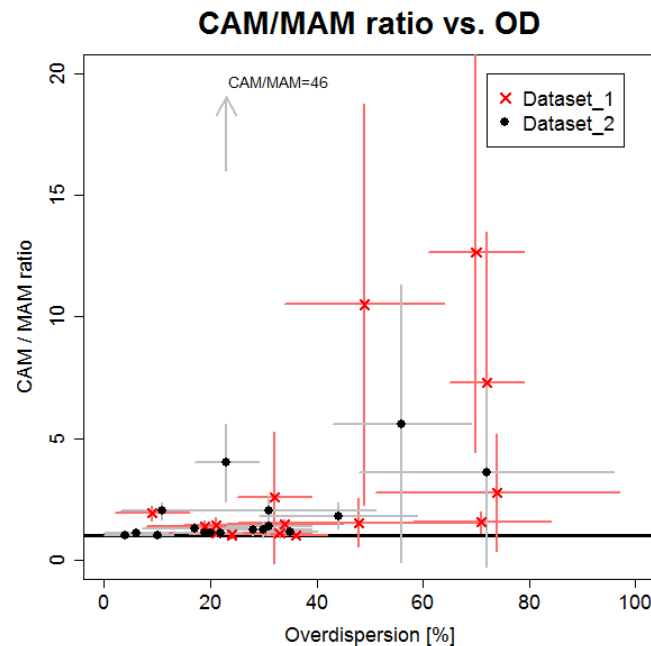

Figure 10: *Scatter plot of the CAM/MAM ratio versus the OD, which presents the differences between these two age models. A higher ratio can be associated with a higher OD. P2_12 with a CAM/MAM ratio of 46 (OD=23) is excluded from the graph.*

4.5. Dose Rate

The DR for the samples in the colluvial horizon range from 2.10 ± 0.10 Gy/ka to 2.65 ± 0.10 Gy/ka (Appendix Table A2). The DR is lower in the fAh of BP5_102 (1.25 ± 0.11 Gy/ka) due to high organic matter and water contents (Appendix Table A2). The cosmic dose rate component for both fAh samples (P2_85 and BP5_102) had been determined as described in Section 3.3. The difference this made for the final age of the samples was small: 20 years in core BP5 and 30 years in pit P2.

4.6. OxCal

The results of the OxCal analysis for P2 (Figure 11A) provide a chronology in stratigraphic order getting older with depth. For P2, almost all samples meet the agreement threshold of 60%. The exception is sample P2_60, which has an agreement factor of 2%. However, the D_e distribution (Figure 9B) shows that this is caused by two outliers and is not supported by the whole distribution. The strong influence of these two outliers that are likely influenced by bioturbation is caused by the use of the MAM age model. Therefore, even though the agreement factor of P2_60 is low (only 2%), it was not removed from the OxCal simulation and the calculated age consequently depended mainly on the modelled likelihood distributions of samples below and above. For P2_70 with only one D_e measurement close to 0Gy, an agreement factor above 100% is still obtained.

Using the OxCal analysis approach for P3 with only two samples gives Priors and Posteriors that are 100% in agreement with each other (Figure 11B). In comparison to P2, the modelled age at 70cm depth is younger, but the ages at 30cm for both sampling locations are very young with roughly 50 years of age (Appendix Table A3).

For the location BP5 in the center of the depression (Figure 11C), the modelled Posteriors are well in agreement with the Priors, and the agreement factors range between 86 and 105%. The largest differences between Priors and Posteriors are found in BP5_82 and BP5_72 where the Priors form a slight age inversion.
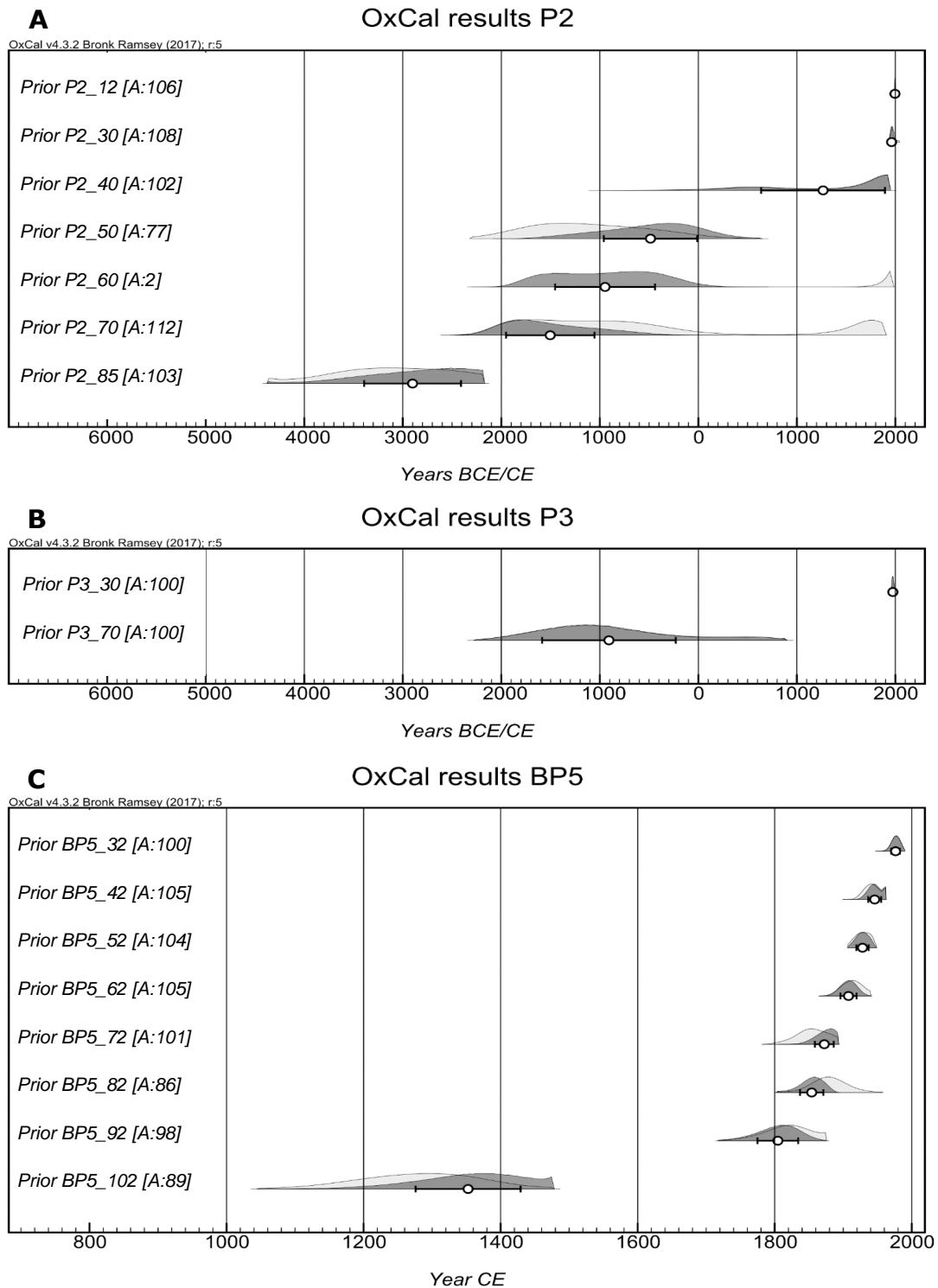

Figure 11: *Ages resulting from the D_e analysis using Bayesian statistics and the OxCal program. Per sampling location, the samples are presented in stratigraphic order. The Priors are presented in light grey and the modelled Posterior distributions in dark grey. Furthermore, the mean and the 1 sigma significance are presented by the white dot and error bars. Next to the sample code, the agreement factor is shown. **A** and **B** give the results from the soil pits P2 and P3, **C** gives the results from core BP5. All but one sample in **A** (P2_60) have agreement factors above the threshold value of 60%.*

16

4.7.   Reliability of the chronologies

A comparison of the different D_e analysis approaches shows the differences in the resulting ages per depth (Figures 12 and 13). Pit P2 shows ages ranging from approximately 5000 years for the fAh to less than 30 years for the Ap (Appendix Table A3). The two samples of P3 show an age of roughly 300 years at 70cm depth and a very young age of about 40 years for P3_30. Compared to P2 and P3, the obtained ages of BP5 are younger with the oldest age being roughly 650 years.
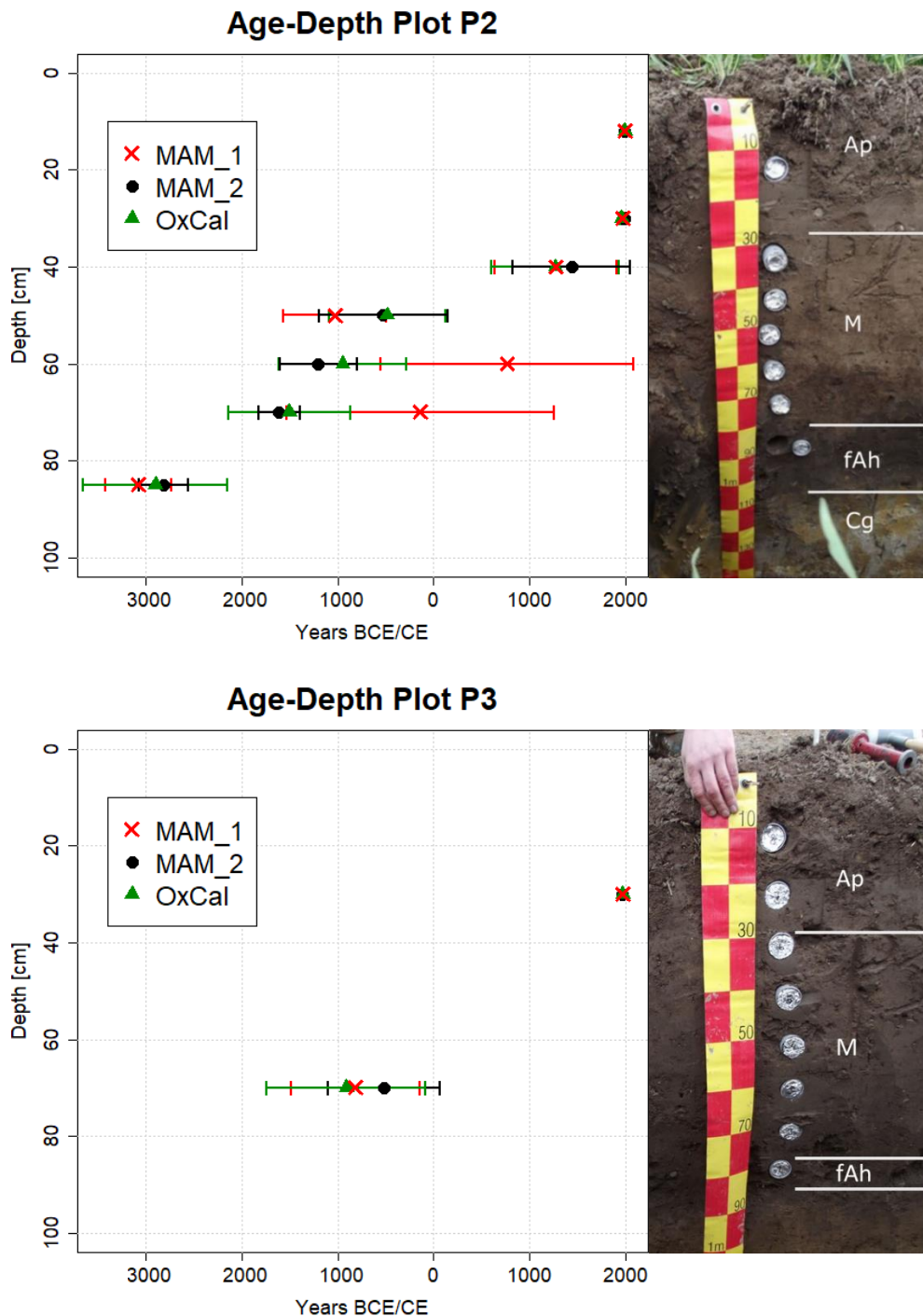

Figure 12: Age-depth plots for pits P2 and P3 comparing the ages resulting from the three different De analysis approaches. MAM_1 represents the age based on the full De Dataset_1, MAM_2 shows the ages resulting from the De Dataset_2 that excludes outliers and OxCal refers to the ages obtained from applying Bayesian statistics and the OxCal program to the full De Dataet_1. The soil profile per sampling location is presented on the right hand side.
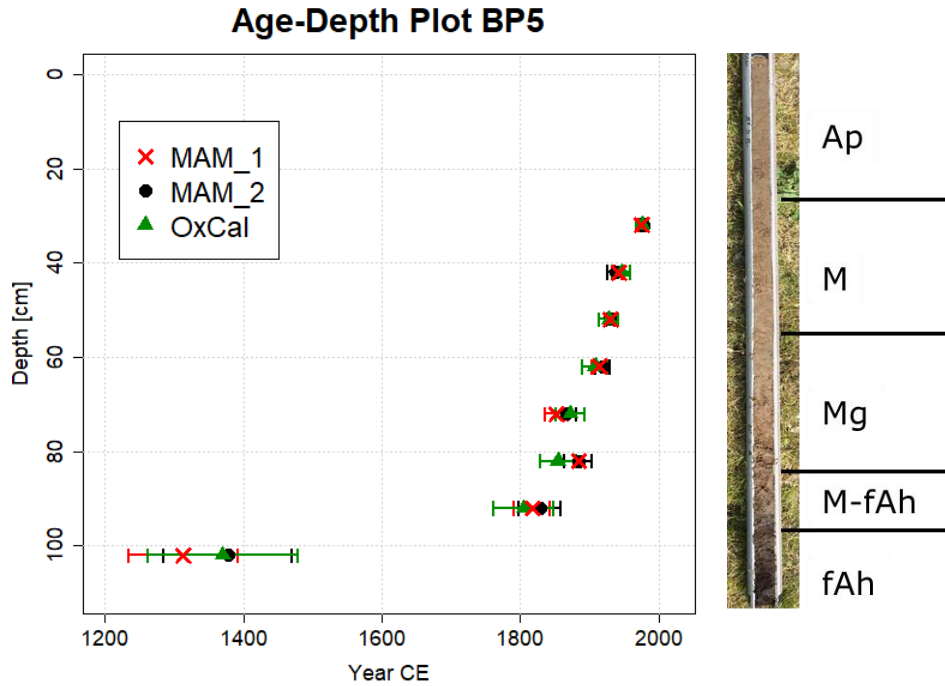
Figure 13: *Age-depth plot for core BP5 comparing the ages resulting from the three different De analysis approaches. MAM_1 represents the age based on the full De Dataset_1, MAM_2 shows the ages resulting from the De Dataset_2 that excludes outliers and OxCal refers to the ages obtained from applying Bayesian statistics and the OxCal program to the full De Dataet_1. The soil profile per sampling location is provided on the right hand side.*

When looking at the MAM_1 ages resulting from the full Dataset_1, it is clear that the ages are not in stratigraphic order, especially for P2_70 and P2_60. For these two samples, MAM_1 provides ages much younger (~1500-2000 years) than those of the other two approaches. This discrepancy can be explained by the strong influence of bioturbated outliers caused by the truncated distribution used in the MAM model (Galbraith et al. 1999). This has also been described for a fluvial setting by Rodnight et al. (2006). Therefore, either outlier removal or the choice of an analysis approach that can deal with outliers on both ends of the D_e distributions is necessary for OSL dating in colluvial sediments. Outlier removal was applied for Dataset_2, and Bayesian statistics were used to obtain the OxCal ages. For the other samples, the differences between the MAM_1 and the MAM_2 ages are small. Notable is that for the fAh in BP5 (BP5_102), the MAM_1 age is slightly higher (~80 years) than the MAM_2 or OxCal ages (Figure 13).

When comparing the MAM_2 ages to the ages resulting from the OxCal approach, the differences in general are small. Both of the approaches can deal with the D_e measurements influenced by bioturbation in P2_60 and P2_70 and the resulting ages show only minor differences for these two samples (Figure 12A). Hence the OxCal results confirm that the choice of 2.5σ for outlier removal was appropriate and on the other hand, the D_e Dataset_2 results confirm the ages obtained through Bayesian statistics and OxCal. Outlier removal, as was performed for D_e Dataset_2, was based on the choice to remove all values falling outside a 2.5σ distribution. 2.5 σ was chosen as it caught most outliers visible to the eye. Therefore, this choice is rather arbitrary and might not necessarily be the best choice for every sample. The OxCal approach deals differently with the outliers, as they are still included in Dataset_1. The Priors strongly depend on the few very young D_e measurements (Figure 11A) due to the MAM. However, due to the stratigraphic order included in OxCal, the large age underestimations of MAM_1 are solved. This is the first advantage of OxCal over the MAM_2 approach. Using the full dataset is methodologically more objective than removing single outliers. However, it is necessary to carefully check whether the samples contain young outliers throughout the profile. If this is the case and a MAM is used, OxCal will shift the entire profile towards these D_e measurements and hence give erroneous age results.

Small age inversions, as found for BP5_82 are only solved by the OxCal approach. The MAM_1 and MAM_2 ages for this sample are both slightly older than the ages of the samples above and below. Due to the

stratigraphic information included in OxCal, this can be resolved. This is the second major advantage of this program, as it is certain that burial ages cannot get younger with depth in this colluvial setting.

Concluding, poor bleaching was observed in this lowland colluvial setting (e.g. Figure 9A) as was expected. The chosen MAM was well supported by the D_e distributions and the CAM/MAM ratio (Figure 10). However, the results made clear that careful attention has to be paid to outliers, especially to young ones. An analysis approach using Bayesian statistics requires the least arbitrary inputs in terms of outlier removal and corresponding thresholds. Therefore using OxCal is the preferred D_e analysis approach and is further used for calculation of the sedimentation rates.

4.8. Sedimentation rates

As described in Section 3.1, the different locations were sampled using different methods: sampling in a soil pit (P2 and P3) and sampling in a soil core (BP5). This was not planned originally and horizontal OSL samples did have the preference. Compaction of the sediment in the core during drilling could have introduced uncertainty in the depth measurements, which is of relevance especially for the sedimentation rates. This could have implications on the OSL ages, as the total thickness of the sediment sampled could have been stretched. As a result of this, the D_e distributions would be broader than they should be for the 5cm thickness chosen. A sign of this happening would be parabolic shapes of horizon boundaries at the core. However, the pictures taken of the core BP5 used for DR measurements do not show signs of parabolic shapes at e.g. the border of the fAh horizon or with the gley features observed in the profile (Appendix Figure A4), and the D_e distributions of BP5 also do not show surprisingly broad distributions (Appendix Figure A3). Moreover, the D_e samples do not include material from directly at the core wall (Figure 6). This gives confidence that the influence of friction at the core walls on sediment layering is small.

The sedimentation rates calculated for the three different profiles show a number of differences, with the sampling depth as well as the sample age (Figures 14 and 15). The sedimentation rates of P2 and P3 show a clear contrast between the upper part of the soil profile (30cm and higher) and the lower part. The highest sedimentation rates are found in the upper part of the profiles which is influenced by constant mixing in the current Ap and constant bioturbation which decreases rapidly with depth (Reimann et al. 2017). The lower part of the P2 and P3 profiles shows very low sedimentation rates, that fall together with the high ages of these samples (Figure 15). Although these sedimentation rates all are very low, they still vary slightly with depth. For P2, the sedimentation rates of the lower three samples show a slight increase with decreasing depth followed by a small decrease that falls roughly falls between 5000 BCE and 1250 CE. This sedimentation rate is also the smallest with 6cm in 1000 years (Appendix Table A3). The younger samples located at shallower depth show higher sedimentation rates.

The calculated sedimentation rates for core BP5 are much higher than those calculated for the lower parts of the P2 and P3 profiles (Figure 14). Only the sedimentation rate between the fAh and the first colluvial sample in BP5 (BP5_102 and BP5_92) is of comparable magnitude to the rates obtained for P2 and P3. The high sedimentation rates found since the beginning of the 19th century match the hypothesis of increased sedimentation since the mechanization of agriculture. Due to the high sedimentation rates, the impact of bioturbation in BP5 is lower than in the slowly deposited colluvium on P2 and P3 (Bateman et al. 2003). The sedimentation rates of BP5 further show a less clear pattern than P2 and P3, with several jumps and larger uncertainties (Figure 13). The major contribution to this sedimentation rate error comes from the uncertainties in age of the samples, the depth error of 1cm has only a minor contribution to the total sedimentation rate error. Further discrimination of phases in sedimentation rate within the past 200 years is not possible due to the high uncertainties and the close spacing of the samples in both depth and age. The described jumps are much less visible when plotting sedimentation rates against the ages of the samples (Figure 15), as the ages of the samples in BP5 lie together very close.
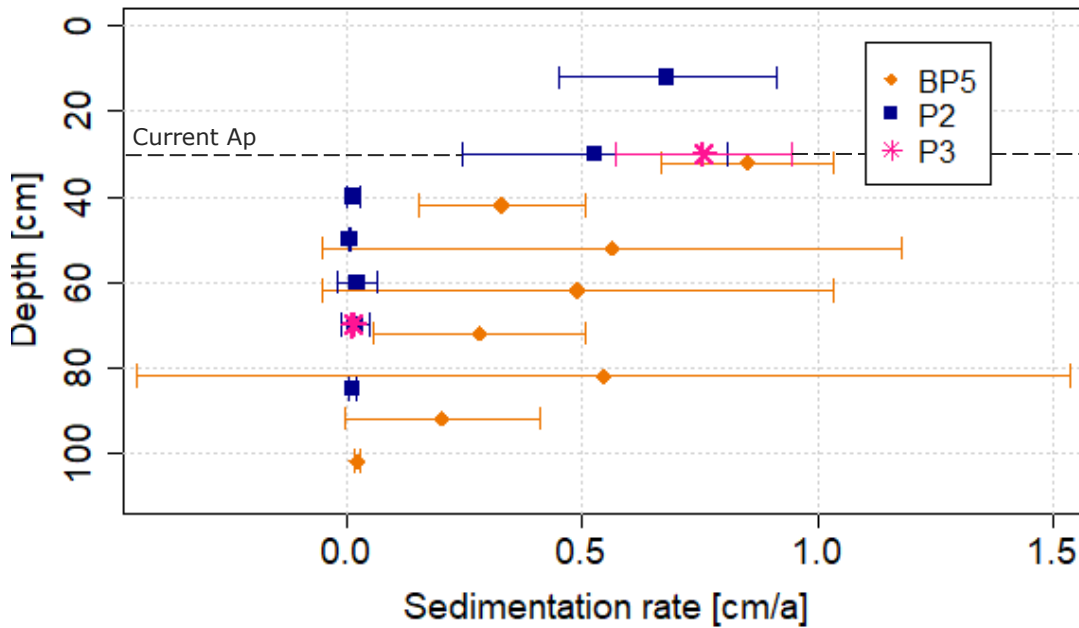
Figure 14: *Sedimentation rates per depth for the three profiles, based on the OxCal age results. The depths are the depth of the lower sample used for the corresponding sedimentation rate. The uppermost sedimentation rate is based on a surface depth of 0cm and surface age of 0 years.*
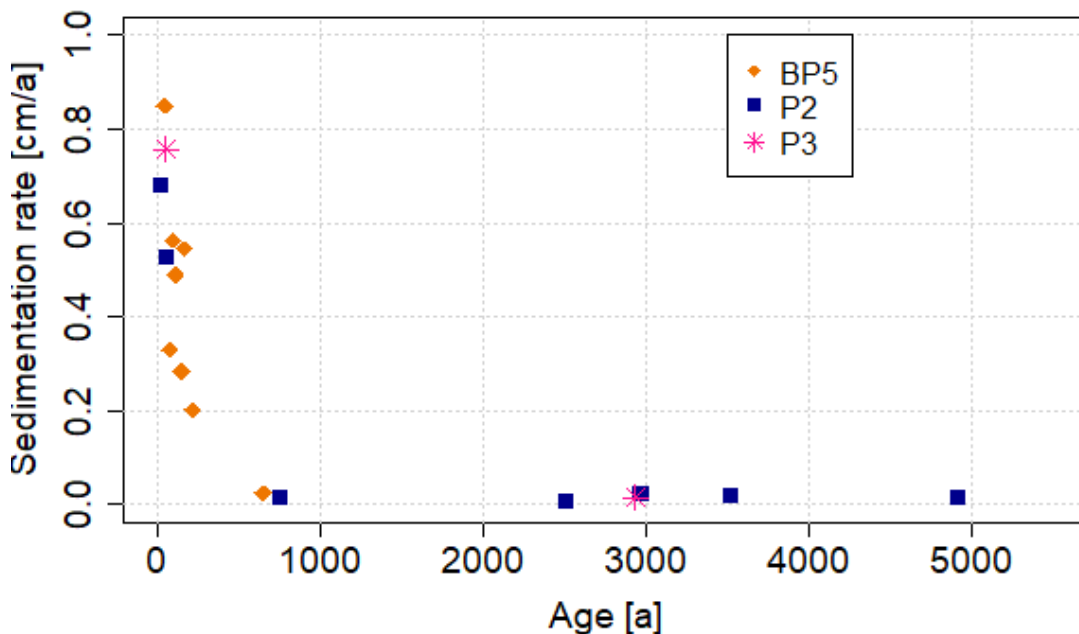

Figure 15: *Sedimentation rates plotted against the ages of the samples. The lower rates correspond to the higher ages of P2, P3 and the fAh of BP5. The exception to this are the young samples of P2 and P3, that have high sedimentation rates and are located in or just below the ploughing layer. Errors are excluded for clarity reasons, but can be seen in Figure 14.*

Sedimentation rates have previously been studied by using ^{137}Cs and radiocarbon dating of the fAh concluding that rates after 1955 were higher than before (Kleeberg et al. 2016; Frielinghaus and Vahrson 1998). For BP5, which is the sampling location that covers the age ranges used in these previous studies, also average sedimentation rates were calculated for comparison. These are roughly 0.1 cm/a between the fAh from the Middle Ages and the sample closest to 1955 CE in age (BP5_42). Higher up in the profile, the averaged sedimentation rate until the surface with an age of zero is ~ 0.6 cm/a. This higher sedimentation rate after 1955 CE is in agreement with the previous studies by Kleeberg et al. (2016) and Frielinghaus and Vahrson (1998). The dating with OSL however provides more differentiated sedimentation rates over time, as it is not restricted to the mid-1950s when nuclear weapon testing started, releasing ^{137}Cs into the environment (Mabit et al. 2008). In the CarboZALF-D kettle hole, Aldana Jague et al. (2016) found that based on ^{137}Cs, a maximum of 27cm was deposited between 1954 and 2011 CE. According to the OSL ages in BP5, the year 1954 should be situated between 32cm and 42cm depth, which is slightly lower than the findings of Aldana Jague et al. (2016).

4.9.   Transport processes

It was expected that if different transport processes, e.g. water and tillage erosion, contributed to soil redistribution, this would be visible in the measured D_e distributions. A sample's OD depends on how much of the D_e distribution is not explained by the experimental uncertainties (Arnold et al. 2009; Lian and Roberts 2006), and hence should provide an indication of the bleaching of the grains prior to deposition. The older samples have been transported mainly by water erosion. The ODs obtained from D_e Dataset_1 were plotted against the age of the samples and the sedimentation rate (Figures 16 and 17). Neither graph reveals a clear relation of the OD with age or sedimentation rate, which contrasts the expectation. The highest D_e measurements are found only in P2 and P3 at the edge of the colluvium (e.g. Figure 9A, Appendix Figures A1, A2 and A3), however this is not visible in the sample's ODs. This means that the transport process has no major influence on the bleaching of the grains in this lowland colluvial setting. Moreover, this implies that bleaching by bioturbation prior to erosion is more important.
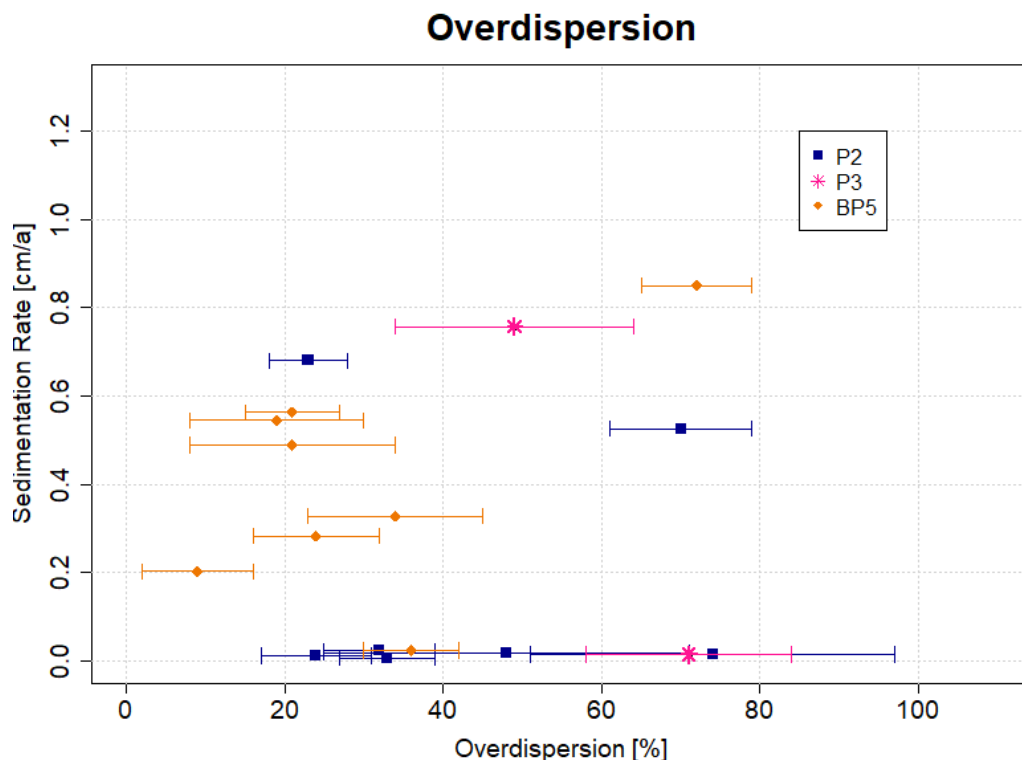

Figure 16: *Graph presenting the overdispersion as a measure of spread in the D_e distribution not explained by experimental uncertainties plotted against the sedimentation rate. The sedimentation rate was determined as described in Section 3.5. The low sedimentation rates belong to the lower part of the P2 and P3 profiles that were not influenced by recent ploughing, and the fAh horizon of BP5 (BP5_102).*
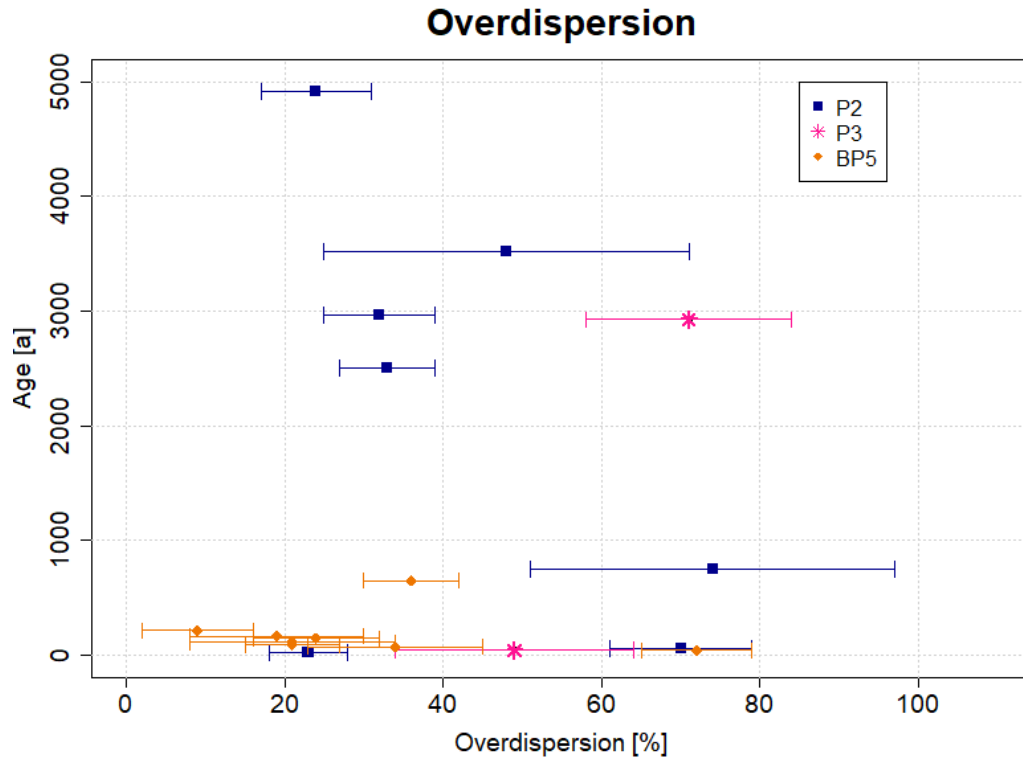
Figure 17: *This graph providing the OxCal ages plotted against the sample overdispersion obtained from the full D_e Dataset_1.*

5. Historical context of colluviation

Information on past land-use around the study area mainly comes from pollen profiles taken from lake sediments (e.g. Jahns 2000, 2001). These pollen records provide land cover information on a regional scale. From the occurrence of cereal pollen or from decreasing amounts of tree pollen, it is possible to determine the presence of human activity and the extent of the natural forest vegetation. Table 2 presents a summary of the information, combined with the ages that were measured in the different soil profiles. All ages determined by OSL dating and thus phases of soil redistribution fall within times of intense human impact like deforestation and intense agricultural use.

Table 2: *A summary of the historical setting and information on land-use of the respective time. The mean and 1 sigma range of the ages are provided on the right hand side, with the two soil pits at the edge of the colluvium and the core in the center of the colluvium separated from each other. Periods of human impact are highlighted in light grey, whereas periods of decreased human activity are represented in white. The age of the oak stem is given alongside the ages of BP5, as is comes from a comparable landscape position. Sources: (Dreibrodt et al. 2010; Dotterweich 2008; Jahns 2000, 2001; Lüthgens et al. 2011; Sommer et al. 2008; Van der Meij et al. 2017; Wolff 2018)*

Historical context	Land cover/ land-use	OSL ages	
		Pits P2 & P3*	Core BP5
~ 18000 BCE	End of Pomeranian stage, region ice free		
~ 8000 BCE	Development closed woodlands		
3200-1900 BCE	Opening of woodland, signs of tillage	2902 ± 755 BCE	
1900-1445 BCE	Low human influence, few records on historical erosion		
1440-500 BCE	Intense human activity, forest clearance	1504 ± 639 BCE 949 ± 667 BCE 910 ± 829 BCE* 486 ± 608 BCE	
~500 BCE-700 CE	Decreased human impact, extensive forest cover		
From 1300 CE on	Intense agriculture, deforestation, frequent reports of colluvial deposits, 1320: 1st documentary note of Dedelow	1267 ± 669 CE	1306 ± 10 CE (oak tree) 1370 ± 109 CE
17th century	30 Year War, destruction of Dedelow		
From 1700 CE on	Development agriculture, mechanization		1804 ± 43 CE 1845 ± 26 CE 1872 ± 21 CE 1908 ± 18 CE 1928 ± 14 CE 1946 ± 13 CE
After 1945	Industrialization of agriculture	1961 ± 17 CE	
1970's & 1980's	Deeper ploughing	1974 ± 10 CE*	1976 ± 9 CE
		1996 ± 7 CE (Ap)	

None of the obtained ages falls clearly into time periods of low human influence (Table 2), like around 1700 BCE or during the Roman Iron Age and Migration Period (Jahns 2001). For these periods there are also elsewhere only few reports on large scale historical soil erosion (Dreibrodt et al. 2010) and they are linked to an extensive woodland coverage (Dotterweich 2008). Therefore it can be concluded that these periods must have been relatively stable, but without forming an A horizon still visible in today's profile. An explanation for this would be that either deposition continued at very low intensity, or that erosion of an A horizon took place when the next phase of intensive land-use started. Next to human impact, climate is also a possible driver for soil erosion and deposition, however human impacts are dominant since Neolithic times (Fuchs 2007). However, human actions are also influenced by climatic conditions, and may on the other hand mask underlying climatic drivers to soil erosion (Zolitschka et al. 2003).

In order to obtain a clear picture of where to place the OSL ages in the landscape development, the results are discussed in three main phases: Firstly the landscape before colluviation started, followed by the slow colluviation that is found in P2 and P3 and finally the rapid colluviation that was found in the results of BP5. Figure 18 provides an illustration of the changes the kettle hole has undergone over time.

5.1.   Prior to colluviation

The fAh sample of P2 (P2_85) is roughly 5000 years old. Since the fAh represents the former land surface (Frielinghaus and Vahrson 1998), bioturbation leads to continuous addition of bleached grains in the sediment (Lang and Hönscheidt 1999). These stable conditions are found in the extensive woodlands present in the region (Jahns 2000), where in absence of erosion and deposition an Ah could form (Emadodin et al. 2011) (Figure 18A). Therefore, the OSL age obtained for this mineral fAh is not the depositional age of the sediment, but rather the moment in time when biological activity shifted upwards, meaning that colluviation on top of the fAh started (Lang and Hönscheidt 1999). The age of 5000 years corresponds to the time period of first reported intense agricultural activity in the Uckermark region with signs of tillage (Jahns 2001) (Table 2).

5.2.   Slow colluviation

Within the colluvial soil horizon, the next group of dates (P2_70, P2_60 and P3_70) falls within the second phase of intense human disturbance combined with reports of forest clearance (Jahns 2000, 2001) (Table 2, Figure 18B and 18C). The next age, P2_40, falls within the Middle Ages, however with a very large uncertainty. This sample also shows a high OD of more than 70% (Appendix, Table A2). Possibly it has been affected by ploughing, if the topmost sedimentation took place in times when ploughing was already present.

In core BP5, the fAh is of organic nature with an organic matter content of 40% (Appendix Table A2). From previous studies it is known that below the fAh, the CarboZALF-D kettle hole hold peat layers (Van der Meij et al. 2017). This is commonly described for kettle holes (Frielinghaus and Vahrson 1998). The OSL age obtained for the fAh of BP5 (BP5_102) represents the start of colluviation in the depression in the 14th century. The pollen profiles that gave information on land-use unfortunately have been disturbed by anthropogenic activities from medieval times onward (Jahns 2001, 2000). During previous sampling activities in the CarboZALF-D site, an oak stem had been found at the base of the colluvium, just above the peat that was dated to have died in 1306 ± 10 CE (Van der Meij et al. 2017). This is slightly older than the onset of colluviation in BP5, within errors however, the ages are in agreement with each other (Table 2). Furthermore, the oak stem is originating from a different sampling location than the samples used for dating. Between the onset of colluviation in the center of the depression and the next OSL age lie a bit more than 400 years. During this time, the plague and war kept the population density low in central Europe (Dotterweich 2008). Dedelow itself had been destroyed during the 30 Year War (Wolff 2018).

Lang and Hönscheidt (1999), who also found younger deposits on the lower slope, explain the delay in lower slope deposition by repeated temporary storage of sediment on the slope followed by erosion, until final deposition. The former landscape before colluviation is described to be rougher (Van der Meij et al. 2017), and smaller sinks at the slopes had to be filled up first (Figure 18B and C). This could explain the different colluvium phases in the study area. It is possible and likely that sediment from the slopes, including the positions of P2 and P3, has been eroded and redeposited in the center of the kettle hole. The timing of this erosion likely took place after the onset of colluviation in the center of the depression.

5.3. Rapid colluviation

The largest part of the meter thick colluvium in the center has been deposited since the beginning of the 19th century (Figure 13, Figure 18D). Due to the position of BP5 in the center of the depression and the peat in the subsoil, it is unlikely that the ground has been ploughed from the beginning of deposition in the 14th century on, due to the wet conditions. However from the time that the depression had filled up enough to be stable for ploughing, this surely was done. The change from an unploughed to a ploughed colluvium in core BP5 should be visible in the sedimentation rates with a lower magnitude. The reason for this is the introduction of younger grains to a depth (30cm) greater than most of the bioturbation (Reimann et al. 2017). Due to the large uncertainties in sedimentation rate, the clear identification of such a jump is not possible (Figure 14). If disregarding the uncertainties, BP5 shows two depths of decreasing sedimentation rate. These are at roughly 70cm and 40cm.

The experimental field at CarboZALF-D is used for a range of studies, including a manipulation experiment during which an extra 5cm of sediment were added onto the field (Deumlich et al. 2017). This experiment affected sampling locations BP5 and P3. Consequently, the P3_30 and BP5_32 actually had been within the ploughing layer until recently (2010). This can also be seen in the resulting ages, as all three, the Ap horizon sample and the two unexpected Ap horizon samples have very similar ages of 21 ± 7a, 41 ± 9a and 43 ± 10a respectively.

P2_30 and P2_12 date to the past 50 years and are in strong contrast to the rest of the profile. Although this is expected for the Ap horizon (P2_12), the young age of 56 ± 17 years of the uppermost colluvium (P2_30) suggests that this depth has also been exposed to recent mixing, most likely by ploughing.
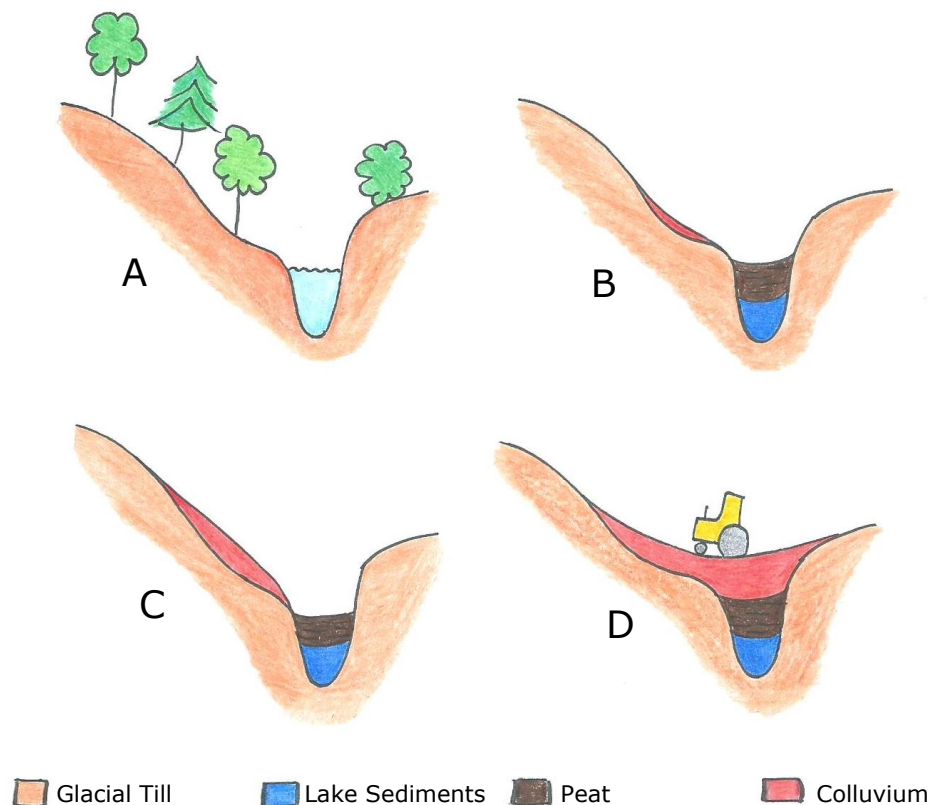

Glacial Till   **Lake Sediments**   **Peat**   **Colluvium**

Figure 18: *Simplified sketch of the main changes in the kettle hole, based on a transect by Van der Meij et al. (2017). After deglaciation, a stable, forested landscape formed (**A**) where slowly lake sediments were deposited in the kettle hole and peat formed (**B**). Deforestation and the initial agricultural use resulted in the first colluviation (**B**) that slowly progressed over time (**C**). Intense colluviation that covered the peat took place in the past centuries under intense agricultural use (**D**). No account was given to vertical and horizontal scaling.*

6. Conclusions

Two soil pits and one core from the colluvium of a lowland kettle hole were dated using OSL. The age results of three different analysis approaches were compared to each other, and sedimentation rates were calculated. The results were used to receive insight into the landscape changes over the past 5000 years.

From the results, the following conclusions can be drawn:

- The use of Bayesian statistics and OxCal presents the best age estimate of the three different analysis approaches. The two main reasons for this are (i) that the program can deal with outliers caused by bioturbation and (ii) that small age inversions in the profile can be resolved due to the stratigraphic information included in OxCal.
- Sedimentation at the edge of the colluvium started around 5000 years ago, with low sedimentation rates. In the center of the depression, the start of colluviation is dated to 1370 CE. Rapid sedimentation occurs from 1800 CE onwards, which can be linked to the mechanization of agriculture.
- The transport process, dominated by water erosion for the older samples and by tillage erosion for the young samples does not seem to influence the D_e distributions. This highlights the importance of bleaching by bioturbation prior to erosion and after deposition.

All the results show that soil redistribution in the CarboZALF-D kettle hole is a complex process influenced by agricultural practices in differing intensities over the past 5000 years. More dating in other locations of the kettle hole will provide further insights into the temporal and spatial aspects of colluviation.

Acknowledgements

Writing this thesis would not have been possible without the support of a number of people. First of all, my thank goes to my supervisors, Tony Reimann and Marijn van der Meij, for offering me the opportunity of this interesting thesis topic. Thanks you for the supervision and feedback throughout the whole process. Moreover, I want to thank Jakob Wallinga, my second supervisor for helping me getting started on the bootstrapped likelihoods. Thank goes also to Cindy Quik, who helped me with finding my way through the OxCal program.

I want to thank Alice Versendaal and Erna Voskuilen from the NCL-laboratory for their help and supervision during the sample preparation and the many measurements.

Furthermore, a big thank to family and friends, who always supported be over the past years in Wageningen, and were there for me in all highs and lows.

References

Aitken, M. J. 1985. *Thermoluminescence dating*: Academic press.

Aldana Jague, E., M. Sommer, N. P. A. Saby, J.-T. Cornelis, B. Van Wesemael, and K. Van Oost. 2016. High resolution characterization of the soil organic carbon depth profile in a soil landscape affected by erosion. *Soil & Tillage Research* 156: 185-193.

Arnold, L. J., R. G. Roberts, R. F. Galbraith, and S. B. DeLong. 2009. A revised burial dose estimation procedure for optical dating of young and modern-age sediments. *Quaternary Geochronology* 4 (4): 306-325.

Bateman, M. D., C. D. Frederick, M. K. Jaiswal, and A. K. Singhvi. 2003. Investigations into the potential effects of pedoturbation on luminescence dating. *Quaternary Science Reviews* 22 (10): 1169-1176.

Bayerl, G. 2006. Geschichte der Landnutzung in der Region Barnim-Uckermark.

BGR. 2015. Bodenübersichtskarte 1 : 200 000 CC3142 Neubrandenburg. Retrieved from https://produktcenter.bgr.de/terraCatalog/Start.do.

Cunningham, A. C., and J. Wallinga. 2012. Realizing the potential of fluvial archives using robust OSL chronologies. *Quaternary Geochronology* 12: 98-106.

Deumlich, D., H. Rogasik, W. Hierold, I. Onasch, L. Völker, and M. Sommer. 2017. The CarboZALF-D manipulation experiment–experimental design and SOC patterns. *International Journal of Environmental & Agricultural Research* 3: 40-50.

Dotterweich, M. 2008. The history of soil erosion and fluvial deposits in small catchments of central Europe: Deciphering the long-term interaction between humans and the environment - A review. *Geomorphology* 101 (1): 192-208.

Dreibrodt, S., C. Lubos, B. Terhorst, B. Damm, and H.-R. Bork. 2010. Historical soil erosion by water in Germany: Scales and archives, chronology, research perspectives. *Quaternary International* 222 (1): 80-95.

Duller, G. A. T. 2008. Single-grain optical dating of Quaternary sediments: why aliquot size matters in luminescence dating. *Boreas* 37 (4): 589-612.

Emadodin, I., S. Reiss, and H. R. Bork. 2011. Colluviation and soil formation as geoindicators to study long-term environmental changes. *Environmental Earth Sciences* 62 (8): 1695-1706.

Frielinghaus, M., and W.-G. Vahrson. 1998. Soil translocation by water erosion from agricultural cropland into wet depressions (morainic kettle holes). *Soil & Tillage Research* 46 (1-2): 23-30.

Fuchs, M. 2007. An assessment of human versus climatic impacts on Holocene soil erosion in NE Peloponnese, Greece. *Quaternary Research* 67 (3): 349-356.

Fuchs, M., M. Fischer, and R. Reverman. 2010. Colluvial and alluvial sediment archives temporally resolved by OSL dating: implications for reconstructing soil erosion. *Quaternary Geochronology* 5 (2): 269-273.

Fuchs, M., and A. Lang. 2009. Luminescence dating of hillslope deposits - A review. *Geomorphology* 109 (1): 17-26.

Galbraith, R. F. 1990. The radial plot: graphical assessment of spread in ages. *International Journal of Radiation Applications and Instrumentation. Part D. Nuclear Tracks and Radiation Measurements* 17 (3): 207-214.

Galbraith, R. F., R. G. Roberts, G. M. Laslett, H. Yoshida, and J. M. Olley. 1999. Optical dating of single and multiple grains of quartz from Jinmium rock shelter, northern Australia: Part I, experimental design and statistical models. *Archaeometry* 41 (2): 339-364.

Godfrey-Smith, D. I., D. J. Huntley, and W.-H. Chen. 1988. Optical dating studies of quartz and feldspar sediment extracts. *Quaternary Science Reviews* 7 (3-4): 373-380.

Guérin, G., N. Mercier, and G. Adamiec. 2011. Dose-rate conversion factors: update. *Ancient TL* 29 (1): 5-8.

Jahns, S. 2000. Late-glacial and Holocene woodland dynamics and land-use history of the Lower Oder valley, north-eastern Germany, based on two, AMS 14 C-dated, pollen profiles. *Vegetation History and Archaeobotany* 9 (2): 111-123.

Jahns, S. 2001. On the Late Pleistocene and Holocene history of vegetation and human impact in the Ücker valley, north-eastern Germany. *Vegetation History and Archaeobotany* 10 (2): 97-104.

Kalettka, T., and C. Rudat. 2006. Hydrogeomorphic types of glacially created kettle holes in North-East Germany. *Limnologica-Ecology and Management of Inland Waters* 36 (1): 54-64.

Kalettka, T., C. Rudat, and J. Quast. 2000. " Potholes" in Northeast German Agro-landscapes: Functions, Land Use Impacts, and Protection Strategies. *Ecological studies*: 291-298.

Kirkels, F. M. S. A., L. H. Cammeraat, and N. J. Kuhn. 2014. The fate of soil organic carbon upon erosion, transport and deposition in agricultural landscapes—A review of different concepts. *Geomorphology* 226: 94-105.

Kleeberg, A., M. Neyen, U.-K. Schkade, T. Kalettka, and G. Lischeid. 2016. Sediment cores from kettle holes in NE Germany reveal recent impacts of agriculture. *Environmental Science and Pollution Research* 23 (8): 7409-7424.

Lang, A., and S. Hönscheidt. 1999. Age and source of colluvial sediments at Vaihingen–Enz, Germany. *Catena* 38 (2): 89-107.

Lian, O. B., and R. G. Roberts. 2006. Dating the Quaternary: progress in luminescence dating of sediments. *Quaternary Science Reviews* 25 (19-20): 2449-2468.

Lüthgens, C., M. Böse, and F. Preusser. 2011. Age of the Pomeranian ice-marginal position in northeastern Germany determined by Optically Stimulated Luminescence (OSL) dating of glaciofluvial sediments. *Boreas* 40 (4): 598-615.

Mabit, L., M. Benmansour, and D. E. Walling. 2008. Comparative advantages and limitations of the fallout radionuclides 137 Cs, 210 Pb ex and 7 Be for assessing soil erosion and sedimentation. *Journal of Environmental Radioactivity* 99 (12): 1799-1807.

Madsen, A. T., and A. S. Murray. 2009. Optically stimulated luminescence dating of young sediments: A review. *Geomorphology* 109 (1): 3-16.

Madsen, A. T., A. S. Murray, T. J. Andersen, M. Pejrup, and H. Breuning-Madsen. 2005. Optically stimulated luminescence dating of young estuarine sediments: a comparison with 210Pb and 137Cs dating. *Marine Geology* 214 (1-3): 251-268.

Maizels, J. K. 1977. Experiments on the origin of kettle-holes. *Journal of Glaciology* 18 (79): 291-304.

Mejdahl, V. 1979. Thermoluminescence dating: Beta-dose attenuation in quartz grains. *Archaeometry* 21 (1): 61-72.

Murray, A. S., and A. G. Wintle. 2003. The single aliquot regenerative dose protocol: potential for improvements in reliability. *Radiation measurements* 37 (4): 377-381.

Prescott, J. R., and J. T. Hutton. 1994. Cosmic ray contributions to dose rates for luminescence and ESR dating: large depths and long-term time variations. *Radiation measurements* 23 (2-3): 497-500.

Preusser, F., D. Degering, M. Fuchs, A. Hilgers, A. Kadereit, N. Klasen, M. Krbetschek, D. Richter, and J. Q. G. Spencer. 2008. Luminescence dating: basics, methods and applications. *Quaternary Science Journal* 57 (1-2): 95-149.

Ramsey, C. B. 1995. Radiocarbon calibration and analysis of stratigraphy: the OxCal program. *Radiocarbon* 37 (2): 425-430.

Ramsey, C. B. 2008. Deposition models for chronological records. *Quaternary Science Reviews* 27 (1-2): 42-60.

Reimann, T., A. Román-Sánchez, T. Vanwalleghem, and J. Wallinga. 2017. Getting a grip on soil reworking–Single-grain feldspar luminescence as a novel tool to quantify soil reworking rates. *Quaternary Geochronology* 42: 1-14.

Rhodes, E. J., C. B. Ramsey, Z. Outram, C. Batt, L. Willis, S. Dockrill, and J. Bond. 2003. Bayesian methods applied to the interpretation of multiple OSL dates: high precision sediment ages from Old Scatness Broch excavations, Shetland Isles. *Quaternary Science Reviews* 22 (10): 1231-1244.

Rodnight, H., G. A. T. Duller, A. G. Wintle, and S. Tooth. 2006. Assessing the reproducibility and accuracy of optical dating of fluvial deposits. *Quaternary Geochronology* 1 (2): 109-120.

Sommer, M., H. H. Gerke, and D. Deumlich. 2008. Modelling soil landscape genesis—a "time split" approach for hummocky agricultural landscapes. *Geoderma* 145 (3): 480-493.

Van der Meij, W. M., A. J. A. M. Temme, J. Wallinga, W. Hierold, and M. Sommer. 2017. Topography reconstruction of eroding landscapes–A case study from a hummocky ground moraine (CarboZALF-D). *Geomorphology* 295: 758-772.

Van Oost, K., W. Van Muysen, G. Govers, J. Deckers, and T. A. Quine. 2005. From water to tillage erosion dominated landform evolution. *Geomorphology* 72 (1-4): 193-203.

Wilkinson, M. T., and G. S. Humphreys. 2005. Exploring pedogenesis via nuclide-based soil production rates and OSL-based bioturbation rates. *Soil Research* 43 (6): 767-779.

Wolff, M. 2018. Dedelow - die Chronik. Retrieved from http://www.dedelow.de/ on February 23, 2018.

Zolitschka, B., K.-E. Behre, and J. Schneider. 2003. Human and climatic impact on the environment as derived from colluvial, fluvial and lacustrine archives—examples from the Bronze Age to the Migration period, Germany. *Quaternary Science Reviews* 22 (1): 81-100.

Appendix

Table A1: *Detailed soil description per sampling location with soil horizo n thicknesses and the depth of the OSL samples that were dated. The Ap horizons pf P3 and BP5, marked with *, have been thickened due to a manipulation experiment by Deumlich et al. (2017), that added 5cm of soil in 2010.*
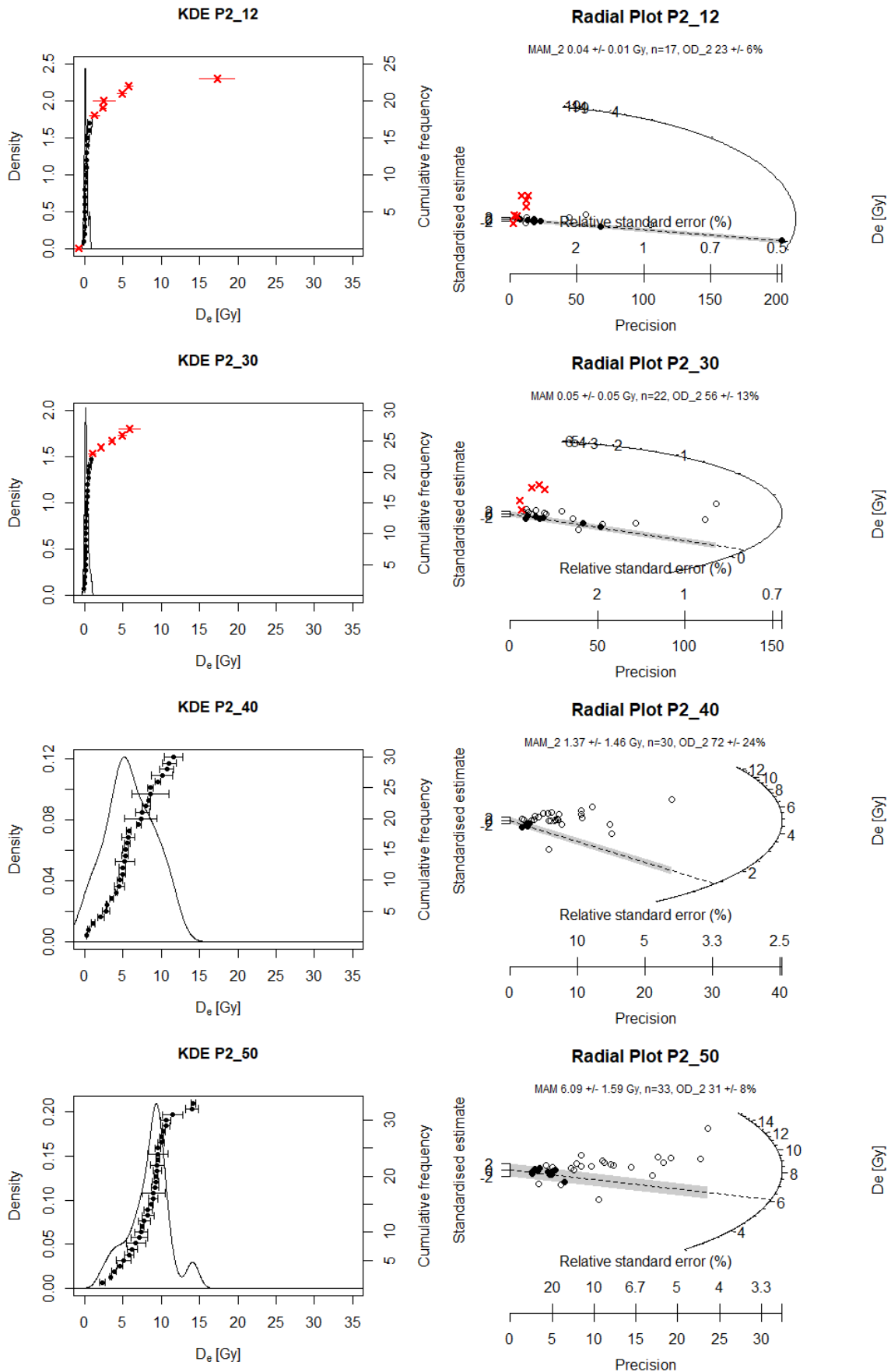
Pit/Core	Horizons [cm]	Depth OSL samples
P2 	0-30: Ap	12cm
	30-45: M	30cm 40cm
	45-65: M-Al	50cm 60cm
	65-75: M-Bt	70cm
	75-110: fAh	85cm
	110-150: Cg	
BP5 *(Photo below)*	0-35: Ap *	32cm
	35-60: M	42cm 52cm
	60-90: Mg	62cm 72cm 82cm
	90-102: M-fAh	92cm
	102-107: fAh	102cm
P3 	0-35: Ap *	30cm
	35-78: M	
	78-85: fAh	70cm
	85-93: Alh	
	93-155: Bt	
	155-165: C	

Figure A1: *KDE- and Radial plots from P2 with the samples provided for increasing depth. Outliers as defined by the outlier removal approach (Section 3.4) are presented with red x. Continuation next page.*
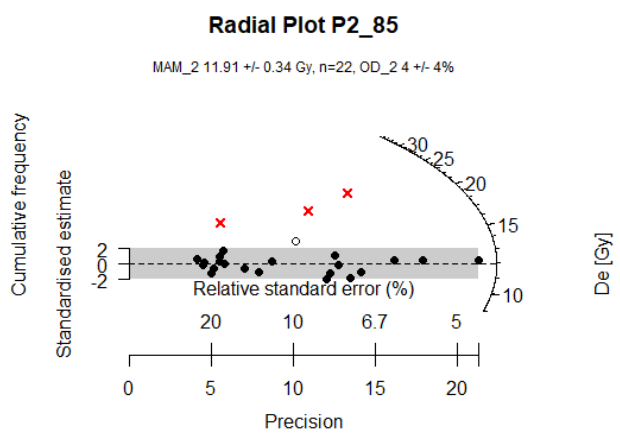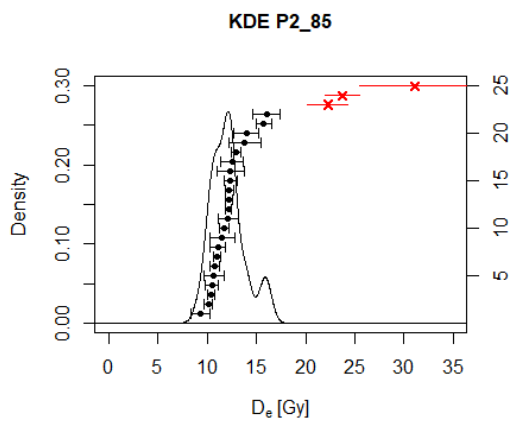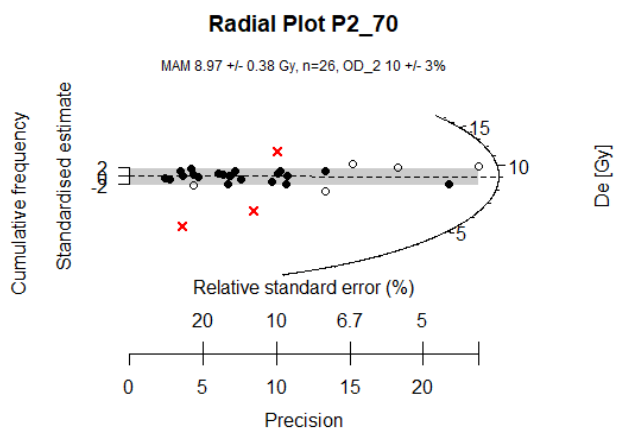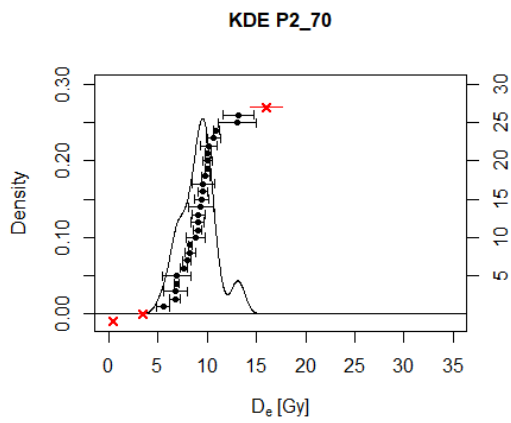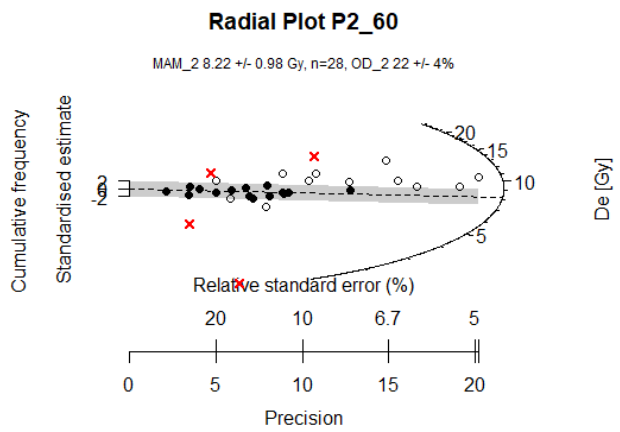
KDE P2_60

Radial Plot P2_60

MAM_2 8.22 +/- 0.98 Gy, n=28, OD_2 22 +/- 4%

KDE P2_70

Radial Plot P2_70

MAM 8.97 +/- 0.38 Gy, n=26, OD_2 10 +/- 3%

KDE P2_85

Radial Plot P2_85
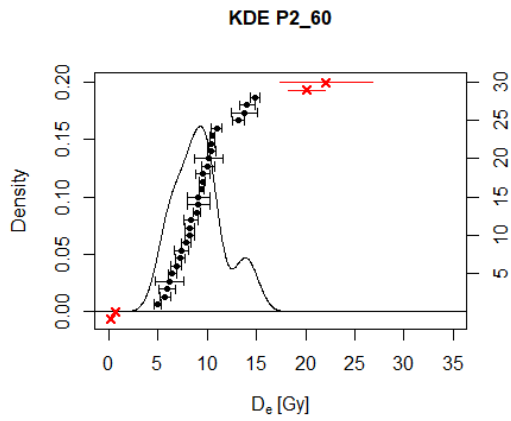
MAM_2 11.91 +/- 0.34 Gy, n=22, OD_2 4 +/- 4%

Figure A2: *KDE plots and Radial plots from P3 with the samples provided for increasing depth. Outliers as defined by the outlier removal approach (Section 3.4) are presented with red x.*

Figure A1: *KDE- and Radial plots from BP5 with the samples provided for increasing depth. Outliers as defined by the outlier removal approach (Section 3.4) are presented with red x. Continuation next page.*
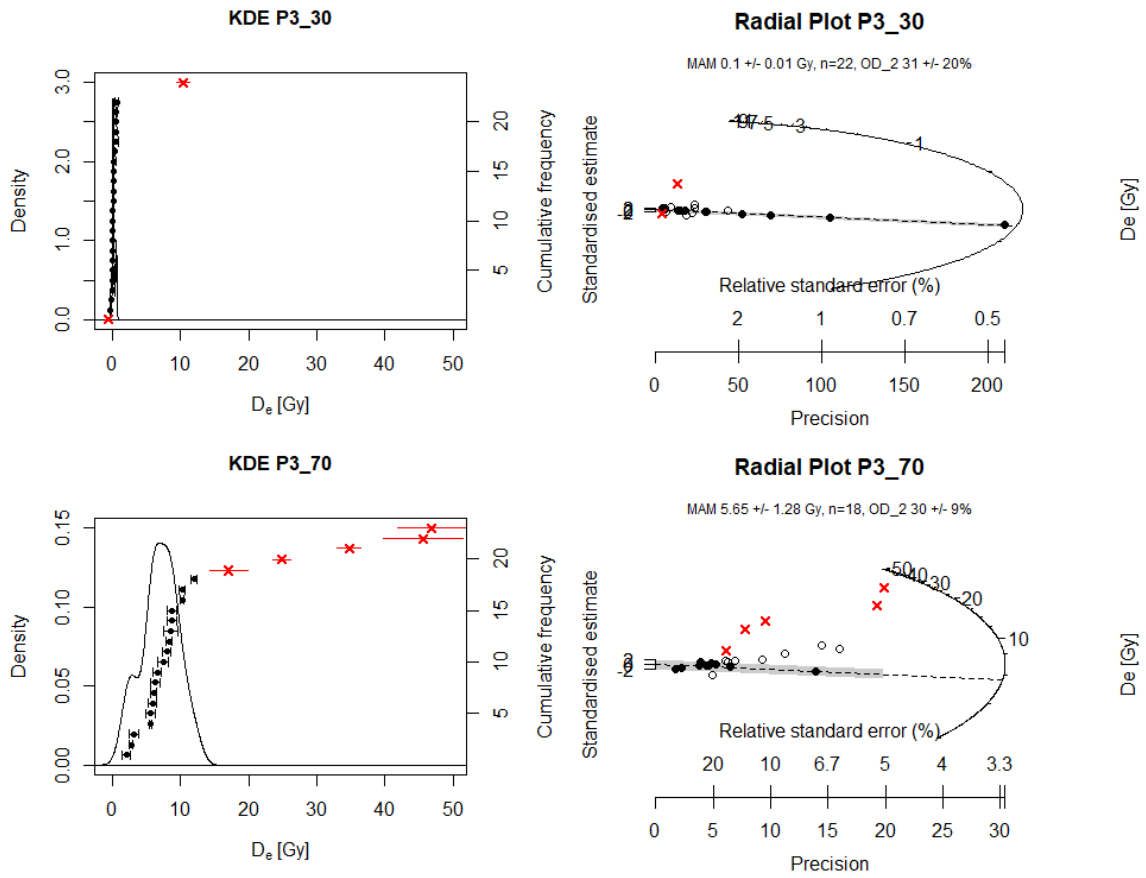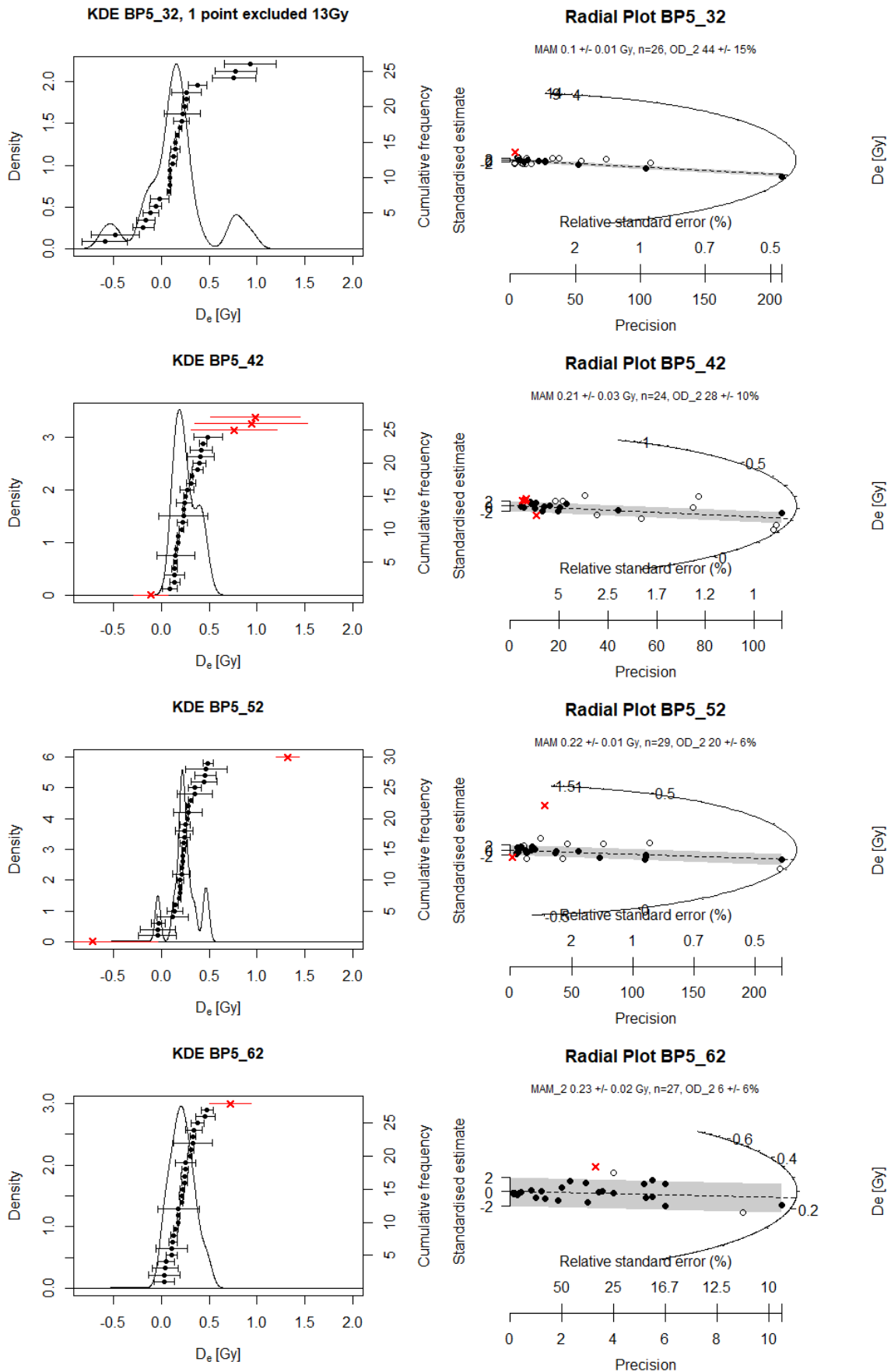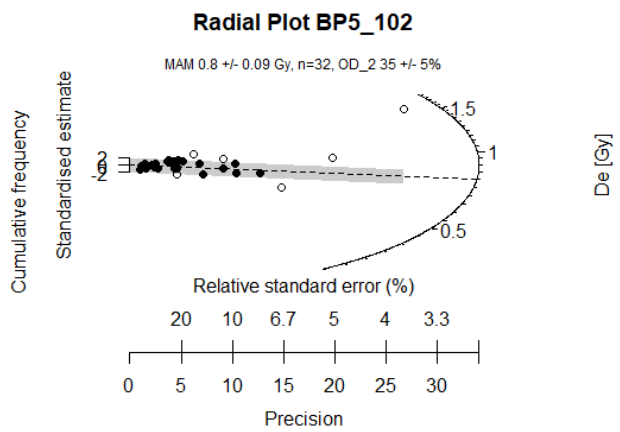
KDE BP5_72

Radial Plot BP5_72

MAM 0.33 +/- 0.03 Gy, n=26, OD_2 19 +/- 6%

KDE BP5_82

Radial Plot BP5_82

MAM 0.28 +/- 0.04 Gy, n=27, OD_2 17 +/- 10%

KDE BP5_92

Radial Plot BP5_92

MAM 0.35 +/- 0.05 Gy, n=32, OD_2 11 +/- 8%

KDE BP5_102

Radial Plot BP5_102

MAM 0.8 +/- 0.09 Gy, n=32, OD_2 35 +/- 5%
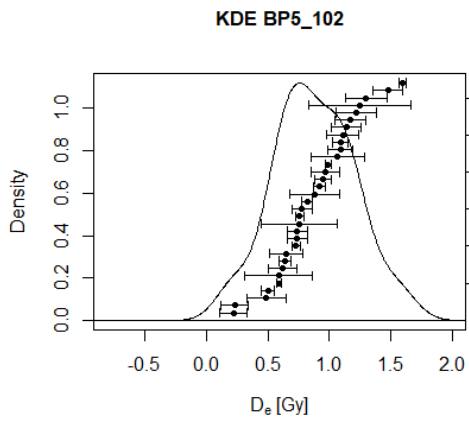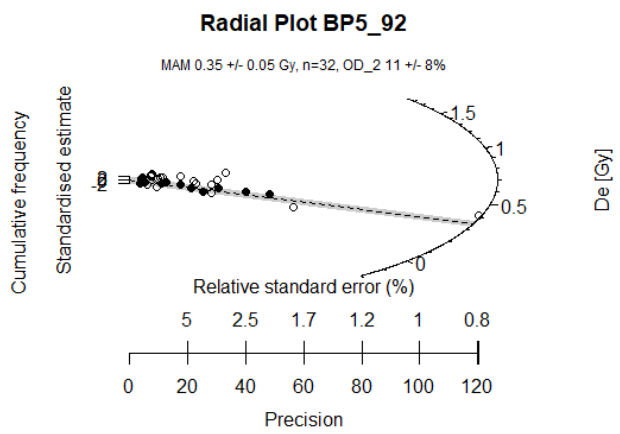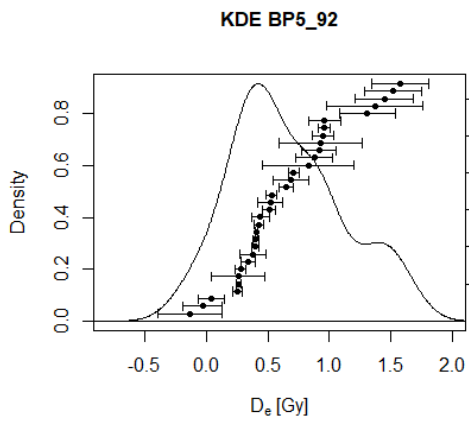
Figure A4: *Photograph the BP5 core that was used for DR measurements. It shows the boundaries between the fAh (>102cm), the transition of fAh to colluvium (M-fAh) (90-102cm) and the colluvium (M) (<90cm), that do not show clear parabolic shapes that would be signs of strong influence of friction at the core wall during sampling.*

Table A2: *Overview of the samples with the laboratory codes, sampling depth and the soil horizon and organic matter and water content that were used for the dose rate calculations.*
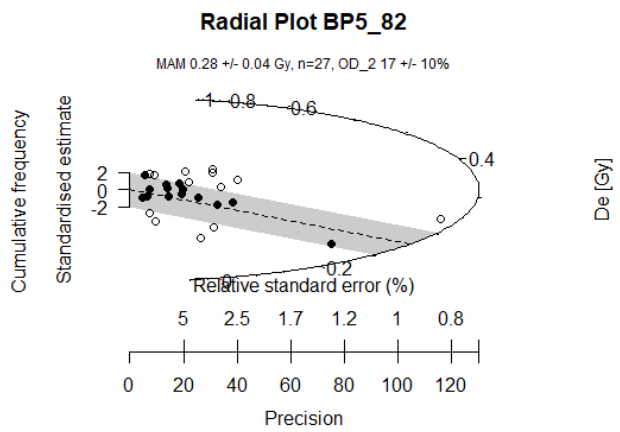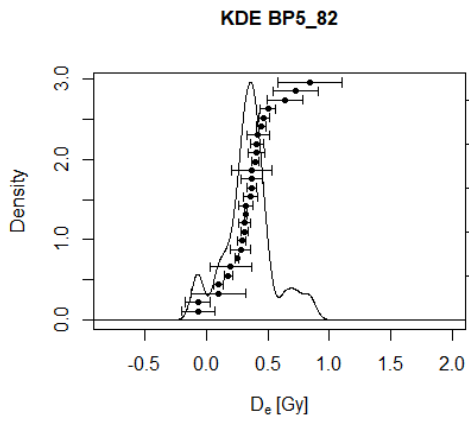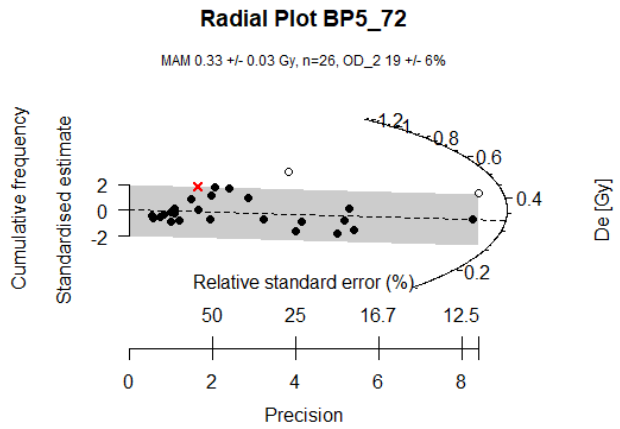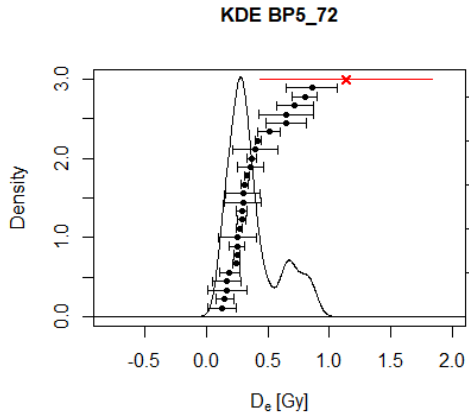
P2

Field Code	NCL Code	Upper depth [cm]	Horizon	OM content [%]	Water content [%]	DR [Gy/ka]
P2_12	NCL-7317068	14.5	Ap	2.4	17.1	2.14 ± 0.09
P2_30	NCL-7317042	32.5	M	2	11.9	2.28 ± 0.08
P2_40	NCL-7317041	42.5	M	1.7	11.8	2.38 ± 0.08
P2_50	NCL-7317040	52.5	M	1.7	16.1	2.40 ± 0.09
P2_60	NCL-7317039	62.5	M	2.1	16.2	2.56 ± 0.10
P2_70	NCL-7317038	72.5	M	2	16.9	2.47 ± 0.10
P2_85	NCL-7317037	87.5	fAh	1.7	18.1	2.47 ± 0.10

P3

Field Code	NCL Code	Upper depth [cm]	Horizon	OM content [%]	Water content [%]	DR [Gy/ka]
P3_30	NCL-7317070	32.5	M	2.2	14.8	2.23 ± 0.08
P3_70	NCL-7317069	72.5	M	2.4	17.1	2.23 ± 0.09

BP5

Field Code	NCL Code	Upper depth [cm]	Horizon	OM content [%]	Water content [%]	DR [Gy/ka]
BP5_32	NCL-7317067	34.5	M	2.7	16.1	2.59 ± 0.10
BP5_42	NCL-7317066	44.5	M	2.8	16.5	2.65 ± 0.10
BP5_52	NCL-7317065	54.5	M	2.6	16.8	2.52 ± 0.10
BP5_62	NCL-7317064	64.5	M	2.4	17.5	2.34 ± 0.09
BP5_72	NCL-7317063	74.5	M	2.5	18.6	2.18 ± 0.09
BP5_82	NCL-7317062	84.5	M	3.6	26.3	2.10 ± 0.10
BP5_92	NCL-7317061	94.5	M-fAh	12	55.7	1.85 ± 0.13
BP5_102	NCL-7317060	104.5	fAh	40.9	152.7	*1.25 ± 0.11**

based on nuclide activities of BP5_92, as no puck could be measured for the fAh sample

Table A2: *Overview of the percentage of accepted aliquots, the ODs from both D_e Datasets per sampling location. Further, the different ages resulting from the three D_e analysis approaches (Section 3.4) are provided, with the best estimate from the OxCal approach marked in grey. The sedimentation rates were calculated as described in Section 3.5.*

P2

Field Code	NCL Code	Aliquots accepted [%]	OD_1	OD_2	Age Model	MAM_1 Age [a]	MAM_2 Age [a]	OxCal age [a]	Sed. rate [cm/a]
P2_12	NCL-7317068	27	23 ± 5	23 ± 6	MAMul	23 ± 9	19 ± 5	21 ± 7	0.680 ± 0.232
P2_30	NCL-7317042	45	70 ± 9	56 ± 13	MAMul	39 ± 22	22 ± 22	56 ± 17	0.526 ± 0.282
P2_40	NCL-7317041	42	74 ± 23	72 ± 24	MAM	739 ± 635	575 ± 614	750 ± 669	0.014 ± 0.014
P2_50	NCL-7317040	41	33 ± 6	31 ± 8	MAM	3045 ± 538	2541 ± 672	2503 ± 608	0.006 ± 0.003
P2_60	NCL-7317039	38	32 ± 7	22 ± 4	MAM	1249 ± 1320	3217 ± 408	2966 ± 667	0.022 ± 0.042
P2_70	NCL-7317038	28	48 ± 23	10 ± 3	MAM	2154 ± 1398	3626 ± 221	3521 ± 639	0.018 ± 0.030
P2_85	NCL-7317037	39	24 ± 7	4 ± 4	MAM	5093 ± 346	4830 ± 257	4919 ± 755	0.011 ± 0.008

P3

Field Code	NCL Code	Aliquots accepted [%]	OD_1	OD_2	Age Model	MAM_1 Age [a]	MAM_2 Age [a]	OxCal age [a]	Sed. rate [cm/a]
P3_30	NCL-7317070	19	49 ± 15	31 ± 20	MAMul	45 ± 5	45 ± 5	43 ± 10	0.757 ± 0.188
P3_70	NCL-7317069	26	71 ± 13	30 ± 9	MAM	2830 ± 671	2534 ± 585	2927 ± 829	0.014 ± 0.004

BP5

Field Code	NCL Code	Aliquots accepted [%]	OD_1	OD_2	Age Model	MAM_1 Age [a]	MAM_2 Age [a]	OxCal age [a]	Sed. rate [cm/a]
BP5_32	NCL-7317067	31	72 ± 7	44 ± 15	MAMul	42 ± 4	39 ± 4	41 ± 9	0.850 ± 0.183
BP5_42	NCL-7317066	33	34 ± 11	28 ± 10	MAMul / MAM *	75 ± 5	79 ± 12	71 ± 13	0.328 ± 0.177
BP5_52	NCL-7317065	37	21 ± 6	20 ± 6	MAMul	87 ± 6	87 ± 6	89 ± 14	0.563 ± 0.615
BP5_62	NCL-7317064	32	21 ± 13	6 ± 6	MAM	103 ± 10	98 ± 10	109 ± 18	0.489 ± 0.542
BP5_72	NCL-7317063	29	24 ± 8	19 ± 6	MAM	165 ± 16	151 ± 15	145 ± 21	0.283 ± 0.225
BP5_82	NCL-7317062	31	19 ± 11	17 ± 10	MAMul	133 ± 20	133 ± 20	163 ± 26	0.545 ± 0.991
BP5_92	NCL-7317061	27	9 ± 7	11 ± 8	MAMul	200 ± 26	189 ± 30	213 ± 43	0.202 ± 0.207
BP5_102	NCL-7317060	21	36 ± 6	35 ±5	MAM	704 ± 79	640 ± 92	647 ± 109	0.023 ± 0.007

* MAMul is used for Dataset_1, MAM is used for Dataset_2 because the negative value is classified as outlier.